A&A 546, A20 (2012)
DOI: 10.1051/0004-6361/201118647

Astronomy & Astrophysics

Galaxy counterparts of intervening high-z sub-DLAs/DLAs and Mg II absorbers towards gamma-ray bursts⋆

S. Schulze[1], J. P. U. Fynbo[2], B. Milvang-Jensen[2], A. Rossi[3], P. Jakobsson[1], C. Ledoux[4], A. De Cia[1], T. Krühler[2], A. Mehner[4], G. Björnsson[1], H.-W. Chen[5], P. M. Vreeswijk[1], D. A. Perley[6], J. Hjorth[2], A. J. Levan[7], N. R. Tanvir[8], S. Ellison[9], P. Møller[10], G. Worseck[11], R. Chapman[1,12], A. Dall'Aglio[13], and G. Letawe[14]

[1] Centre for Astrophysics and Cosmology, Science Institute, University of Iceland, Dunhagi 3, 107 Reykjavík, Iceland
e-mail: sts30@hi.is
[2] Dark Cosmology Centre, Juliane Maries Vej 30, 2100 København Ø, Denmark
[3] Thüringer Landessternwarte Tautenburg, Sternwarte 5, 07778 Tautenburg, Germany
[4] European Southern Observatory, Alonso de CÃşrdova 3107, Vitacura, Casilla 19001, Santiago 19, Chile
[5] Department of Astronomy, University of Chicago, 5640 S. Ellis Ave., Chicago, IL 60637, USA
[6] Department of Astronomy, California Institute of Technology, MC 249-17, 1200 East California Blvd., Pasadena, CA 91125, USA
[7] Department of Physics, University of Warwick, Coventry, CV4 7AL, UK
[8] Department of Physics and Astronomy, University of Leicester, Leicester LE1 7RH, UK
[9] Department of Physics and Astronomy, University of Victoria, Victoria, British Columbia, V8P 1A1, Canada
[10] European Southern Observatory, Karl-Schwarzschildstrasse 2, 85748, Garching, Germany
[11] UCO/Lick Observatory, University of California, 1156 High Street, Santa Cruz, CA 95064, USA
[12] Centre for Astrophysics Research, University of Hertfordshire, Hatfield, Herts AL10 9AB, UK
[13] Astrophysikalisches Institut Potsdam, An der Sternwarte 16, 14482 Potsdam, Germany
[14] Institut d'Astrophysique et Géophysique, Université de Liège, Allée du 6 Août, 17 Bâtiment B5C, 4000 Liège, Belgium

Received 14 December 2011 / Accepted 24 July 2012

ABSTRACT

We present the first search for galaxy counterparts of intervening high-z ($2 < z < 3.6$) sub-damped Lyα absorbers (sub-DLAs) and DLAs towards gamma-ray bursts (GRBs). Our final sample comprises five intervening sub-DLAs and DLAs in four GRB fields. To identify candidate galaxy counterparts of the absorbers we used deep optical- and near-infrared imaging, and low-, mid- and high-resolution spectroscopy acquired with 6-m to 10-m class telescopes, the *Hubble* and the *Spitzer* Space Telescopes. Furthermore, we used the spectroscopic information and spectral-energy-distribution fitting techniques to study them in detail. Our main result is the detection and spectroscopic confirmation of the galaxy counterpart of the intervening DLA at $z = 3.096$ in the field of GRB 070721B ($z_{\rm GRB} = 3.6298$) as proposed by other authors. We also identify good candidates for the galaxy counterparts of the two strong Mg II absorbers at $z = 0.6915$ and 1.4288 towards GRB 050820A ($z_{\rm GRB} = 2.615$). The properties of the detected DLA galaxy are typical for Lyman-break galaxies (LBGs) at similar redshifts; a young, highly star-forming galaxy that shows evidence for a galactic outflow. This supports the hypothesis that a DLA can be the gaseous halo of an LBG. In addition, we report a redshift coincidence of different objects associated with metal lines in the same field, separated by 130–161 kpc. The high detection rate of three correlated structures on a length scale as short as ∼150 kpc in two pairs of lines of sight is intriguing. The absorbers in each of these are most likely not part of the same gravitationally bound structure. They more likely represent groups of galaxies.

Key words. Galaxy: evolution – galaxies: individual: DLA J0212-0211 – quasars: individual: QSO J1408-0346 – gamma-ray burst: general – quasars: absorption lines – Galaxy: formation

1. Introduction

Intervening absorption-line systems found in quasi-stellar object (quasar, QSO) spectra play an important role in the observational study of galaxy formation and evolution. Unlike emission-selected objects, QSO absorption-line systems probe structures over the full mass range from underdense regions to massive virialised dark matter haloes (Rauch 1998; Wolfe et al. 2005). The most neutral-hydrogen-rich absorption systems are called damped Lyα absorbers (DLAs), if the neutral hydrogen column density, N(H I), exceeds 2×10^{20} cm^{-2} ($\log N({\rm H\,I}) \geq 20.3$) and sub-DLAs (or sometimes super-Lyman-limit systems), if the column density in neutral hydrogen is between $\sim 10^{19}$ and 2×10^{20} cm^{-2} (Wolfe et al. 2005, and references therein). The DLAs represent the main reservoir of neutral hydrogen in the

⋆ Based in part on observations collected at the European Organisation for Astronomical Research in the Southern Hemisphere, Chile, as part of the programs 075.A-0603, 075.A-0385, 077.A-0312, 084.A-0303, 177.A-0591 and 275.D-5022. Based in part on observations made with the NASA/ESA *Hubble* Space Telescope, obtained at the Space Telescope Science Institute, which is operated by the Association of Universities for Research in Astronomy, Inc., under NASA contract NAS 5-26555. Based in part on observations made with the *Spitzer* Space Telescope, which is operated by the Jet Propulsion Laboratory, California Institute of Technology, under a contract with NASA. Based in part on observations obtained at the Gemini Observatory, which is operated by the Association of Universities for Research in Astronomy, Inc., under a co-operative agreement with the NSF on behalf of the Gemini partnership.

high-z ($z > 2$) Universe (Wolfe 1986; Péroux et al. 2005; Wolfe et al. 2005). Since the advent of QSO absorption-line spectroscopy, over 1000 intervening sub-DLAs and DLAs have been detected (Prochaska et al. 2005; Noterdaeme et al. 2009; Prochaska & Wolfe 2009).

Although their frequency and chemical composition are well known, the nature of their galaxy counterparts (hereafter called DLA galaxies) has remained poorly constrained for many years. Various models for DLA galaxies exist: e.g. rapidly-rotating proto-galactic disks at high redshift (Prochaska & Wolfe 1997, 1998; Wolfe & Prochaska 1998), low surface brightness galaxies (Jimenez et al. 1999), faint and small gas-rich dwarf galaxies (Tyson 1988; Haehnelt et al. 1998; Okoshi & Nagashima 2005), compact galaxies (Nagamine et al. 2007), and gaseous haloes of high-z LBGs (Fynbo et al. 1999; Møller et al. 2002; Fynbo et al. 2008; Rafelski et al. 2011). Chen & Lanzetta (2003) showed that the majority of low-z sub-DLAs and DLAs are late-type galaxies and only a few are elliptical or dwarf galaxies. The conclusion that these low-z absorbers are indeed sub-DLAs or DLAs is drawn indirectly. Below $z \lesssim 1.5$, the Lyα absorption line is below 3000 Å, a spectral range that is inaccessible with ground-based telescopes. Ellison (2006) showed that Mg II absorbers with $EW_{\rm rest}$(Mg II λ2796) $\geq$ 1 Å, so-called strong Mg II absorbers, are likely sub-DLAs or DLAs (see also Rao & Turnshek 2000; Ellison et al. 2009).

The successfully identified DLA galaxies allow the study of objects at the very faint end of the galaxy luminosity function (LF), objects that are usually missed in galaxy surveys. During the past 25 years, several deep-imaging campaigns have been carried out, but only with limited success (e.g. Smith et al. 1989; Djorgovski et al. 1996; Le Brun et al. 1997; Fynbo et al. 1999; Warren et al. 2001; Møller et al. 2002; Fumagalli et al. 2010; see also Bouché et al. 2012). Up to now, only about 17 sub-DLA and DLA galaxies have been identified below the redshift of unity (e.g. Péroux et al. 2011, and reference therein) and more than 80 DLA galaxy candidates have been reported to date (e.g. Rao et al. 2011). For the majority of these DLA galaxy candidates there is no spectroscopic confirmation yet. At high redshift the situation is worse; only nine intervening sub-DLAs and DLAs with redshifts between 2 and 3.15 have a confirmed galaxy counterpart (high-z; Djorgovski et al. 1996; Møller et al. 2002; Christensen et al. 2004b; Møller et al. 2004; Weatherley et al. 2005; Fynbo et al. 2010, 2011; Péroux et al. 2012; Bouché et al. 2012; Krogager et al. 2012; Noterdaeme et al. 2012, and references therein). In addition to those, a few associated DLAs, i.e. $z_{\rm abs} \approx z_{\rm em}$, have detected galaxy counterparts (e.g. Fynbo et al. 1999; Møller & Warren 1993; Ellison et al. 2002; Møller et al. 2004; Adelberger et al. 2006).

Apart from the faintness of the galaxy counterparts, another problem that hampers the search for DLA galaxies is the glare of the bright background QSOs. Counterparts with a small angular distance from the QSO (impact parameter) are difficult to recover. This may lead to a possible misidentification of the DLA galaxy and hence to an overestimation of its size, because DLAs at small impact parameters are easily missed. A different class of background light sources, gamma-ray bursts (GRBs), provide a complementary approach to the problem. A GRB is a transient phenomenon, outshining the known Universe in γ-rays for a fraction of a second up to hundreds of seconds (e.g. Kouveliotou et al. 1993; Zhang & Mészáros 2004). This short-lived emission is followed by an afterglow that can usually be detected from the X-rays over optical/near-infrared (NIR) wavelengths to the radio for several weeks (e.g. Racusin et al. 2009; Kann et al. 2010; Chandra & Frail 2012). An afterglow can outshine the brightest quasars by several orders of magnitudes, but only for a very short period of time (~1 h–~1 day; e.g. Bloom et al. 2009; Kann et al. 2010). Similar to QSOs, GRBs can be found throughout most of the observable Universe, the most distant spectroscopically confirmed burst being GRB 090423 at $z \sim 8.3$ (Tanvir et al. 2009; Salvaterra et al. 2009). Indeed, since most GRBs are associated with the death of massive stars (Hjorth & Bloom 2011; Woosley 2011), this should allow us to detect them at higher redshifts than QSOs. In short, GRB afterglows can be brighter than QSOs but they are ephemeral, i.e. they vanish within a couple of months. This leaves the line-of-sight clear and without any interference from a bright object (e.g. Masetti et al. 2003; Vreeswijk et al. 2003; Jakobsson et al. 2004; Ellison et al. 2006; Prochter et al. 2006; Henriksen 2008; Pollack et al. 2009).

Gamma-ray bursts are important for DLA studies for another reason. Nearly all GRB host galaxies have a DLA (GRB-DLA; Fynbo et al. 2009). The distribution of their H I column density and their metal-line strength distributions of Si II λ1526 and C IV $\lambda\lambda$1548&1550 overlap with those of intervening DLAs, but also extend to higher values (Prochaska et al. 2007b; Fynbo et al. 2009). On average GRB-DLAs have higher metallicities than intervening DLAs (Fynbo et al. 2006; Prochaska et al. 2007b; Fynbo et al. 2008). The difference between in situ and intervening DLAs lies in the way they probe their host galaxies (Vreeswijk et al. 2004; Prochaska et al. 2007b; Fynbo et al. 2008, 2009). Because GRBs are thought to originate from the collapse of a massive star, GRB-DLAs probe the line of sight to the location of a massive star, irrespective of the DLA orientation relative to the host galaxy if the progenitor is located in the DLA. Consequently, GRB-DLAs are selected by their star-formation rate (SFR). In contrast, the properties of an intervening DLA depend on the geometry of the DLA galaxy and its orientation relative to the line of sight. These are selected by their covering fraction and hence their cross-section, σ(H I). A debated question in observational galaxy formation and evolution is the faint-end slope of the $z \sim 3$ galaxy LF. The DLA galaxies probe the faint-end slope, but the in-situ and intervening DLA LFs are only identical if σ(H I) $\propto$ SFR (Chen et al. 2000; Fynbo et al. 2008). The studies of both DLA populations therefore complement each other well.

Currently, seven intervening sub-DLAs and DLAs have been found in six GRB afterglow spectra, with absorber redshifts ranging between 2.077 and 3.564 (GRBs 050730, 050820A, 050908, 050922C, 060607A, 070721B; Chen et al. 2005; Fox et al. 2008; Piranomonte et al. 2008; Chen et al. 2009; Fynbo et al. 2009; Vergani et al. 2009). Although the number of intervening (sub-)DLAs towards GRBs does not increase the number of known (sub-) DLAs significantly, the transient nature of the background afterglow simplifies the search for their galaxy counterparts. After the afterglow has faded, deep follow-up observations are usually carried out to find the GRB host galaxy, typically reaching a limiting magnitude of ~27 mag in the R-band (e.g. Hjorth et al. 2012; Malesani et al., in prep.). These observations are also suitable for the search for DLA galaxies.

In this paper we present the findings from our search for the photometric counterparts of intervening sub-DLAs and DLAs in six GRB lines of sight. In Sect. 2, we introduce our methodology, present the sample selection, and describe how the data were reduced. The results are then presented in Sect. 3, confronted with current models of sub-DLAs and DLAs, and compared to low-z and high-z DLA galaxies in Sect. 4. In Sect. 5 we draw our conclusions.

Throughout the paper we refer to the solar abundance compiled in Asplund et al. (2009) and adopt cm^{-2} as the linear unit of column densities, N. We assume a ΛCDM cosmology with $H_0 = 71\,\mathrm{km\,s^{-1}\,Mpc^{-1}}$, $\Omega_\mathrm{m} = 0.27$, and $\Omega_\Lambda = 0.73$ (Larson et al. 2011).

2. Data gathering and reduction

2.1. Sample selection and data gathering

All six GRBs with intervening sub-DLAs and DLAs were part of deep-imaging campaigns dedicated to detect their host galaxies. Among these, we selected those that had sufficient spectroscopic data, e.g. spectra obtained with different position angles (PAs), or multi-filter data to construct the spectral energy distribution (SED) of candidates and determine their nature. This reduced the set to GRBs 050730, 050820A, 050908 and 070721B.

In the following, we briefly describe the photometric and spectroscopic data analysed, as summarised in Table 1. The observing conditions during Keck and *Magellan* observations are described in Chen et al. (2009), while those of other ground-based observations are summarised in Table 1. The astrometric uncertainty is ∼0.″3; the uncertainty between the optical and NIR astrometry is similar, allowing us to unambiguously identify objects in the different bands

2.1.1. GRB 050730

Afterglow spectra of GRB 050730 were acquired with VLT/FORS2 with the 300V grating and with VLT/UVES with the red and blue arm centred at 3460 Å and 5800 Å, respectively (see Table 1). In addition, another spectrum was acquired with VLT/FORS1 (grating 600V; PA = 22.5°), as part of the TOUGH (The Optically Unbiased GRB Host) survey (Hjorth et al. 2012) and three additional spectra with VLT/FORS2 (PI: Ellison; Table 1). For these, the slits were centred on the afterglow position, and spectra with different slit orientations were obtained with the 600B grism. In doing so, most of the field of view close to the GRB position is covered, including several of the brightest close-by objects. This strategy enables us to localise emission line objects via triangulation, similar to Møller et al. (2004), Fynbo et al. (2010), Fynbo et al. (2011), Krogager et al. (2012), Noterdaeme et al. (2012)[1]. Fynbo et al. (2009) reported the serendipitous discovery of a quasar at the same redshift as the intervening sub-DLA towards GRB 050730, 17.″5 south of the afterglow position. The quasar is blended with a 18.2-mag bright foreground star. To investigate the QSO-sub-DLA connection and to constrain the quasar radiation field, we acquired a spectrum of the quasar with VLT/X-shooter (Table 1). The field was also the target of deep imaging campaigns with VLT/FORS2 (R-band) and VLT/ISAAC (K_s-band) as a part of the TOUGH survey (Hjorth et al. 2012), HST/ACS ($F775W$-band, PI: Levan) and *Spitzer*/IRAC (3.6 and 5.8 μm; Table 1).

2.1.2. GRB 050820A

Similar to GRB 050730, GRB 050820A was a target of an extensive spectroscopic campaign. After the afterglow faded, several spectra were acquired with VLT/FORS2 by centring the slit on the afterglow position and using three different slit orientations, each one observed with two different gratings (300V and 1028z; PI: Ellison), see Table 1. Slits were oriented to cover most of the area around the afterglow position and several of the brightest objects close to the afterglow position. The total integration time of the data acquired with the 1028z grism is only half of the time spent on 300V, and the 1028z spectral range does not extend the range of the 300V data substantially, but its resolution is much higher than that of the 300V data. Hence, we did not use the 1028z data in our analysis. In addition, the field was observed in nine filters extending from 473.1 nm (g' band) to 5.8 μm with VLT/FORS2 and VLT/ISAAC as a part of the TOUGH survey, HST/ACS, Keck/LRIS, *Magellan*/PANIC, and *Spitzer*/IRAC (Table 1).

2.1.3. GRB 050908

For this burst, only few data are available. An afterglow spectrum was obtained with the 300V grating (slit width of 1.″0 and PA = 0.°0) using VLT/FORS1, and with Gemini/GMOS-N using the B600 grating (slit width of 0.″75 and PA = 110.°0; Table 1). In addition to these data, we included a spectrum obtained with VLT/FORS1 (600B) and deep R- and K_s-band images acquired with VLT/FORS2 and VLT/ISAAC as a part of the TOUGH survey, respectively, and deep *Spitzer*/IRAC images acquired at 3.6 and 5.8 μm (Table 1).

2.1.4. GRB 070721B

We used the afterglow spectrum (PA = −118.°3) acquired with VLT/FORS2 (Table 1), and a spectrum obtained with VLT/FORS1 (PA = −118.°5) several months after the GRB faded as a part of the TOUGH campaign. In addition, several deep-imaging campaigns targeted this field. We used the VLT/FORS2 R-band and VLT/ISAAC K_s-band data acquired as part of the TOUGH campaign, HST/ACS F775W-band data, and *Magellan*/PANIC H-band data.

2.2. Data reduction

2.2.1. Imaging

Ground-based data – VLT/FORS and Keck/LRIS data were reduced in a standard way, VLT/FORS data with `IRAF` and Keck/LRIS data with `IDL` (Tody 1986; see Malesani et al., in prep. for more details on the VLT data reduction, and Perley et al., in prep., on the Keck data reduction). The NIR data acquired with VLT/ISAAC were reduced in a standard way with the `jitter` routine in `eclipse` (Devillard 1997). The reduction of the *Magellan*/PANIC data is presented in Chen et al. (2009).

HST data – HST/ACS images of GRB 050730 and 070721B consist of six dithered exposures in the $F775W$ filter. Individual exposures, after standard "on-the-fly" processing, were retrieved from the STScI archive[2]. These were subsequently cleaned for bias striping, introduced due to the replacement electronics after Servicing Mission 4 (May 11–24, 2009), and then drizzled using the `multidrizzle` software into final science images. At this stage we adopted a pixel scale of 0.″033, approximately two thirds of the native pixel scale. The data reduction of the GRB 050820A HST data is presented in Chen et al. (2009). The

[1] In fact, the galaxy counterparts of most sub-DLAs and DLAs at $z > 2$ were detected via triangulation.

[2] `http://archive.stsci.edu`

Table 1. Summary of photometric and spectroscopic data.

Photometry[a]					Spectroscopy[b]								
Instrument	Filter	Exposure time (s)	Seeing	Photo-metric?	Instrument	Grating	Spectral range (Å)	Resolving power	Exposure time (s)	Slit width	Position angle	Seeing	Photo-metric?
GRB 050730: RA = $14^h08^m17^s.11$, Dec = $-03°46'17''.70$ (J2000)													
VLT/FORS2	*R*	8 × 250 + 24 × 300	0.″6	yes	VLT/FORS1	600V+GG435	4430–7370	990	5 × 1316	1.″3	22.°5	0.″8	yes
HST/ACS	*F775W*	6 × 1307			VLT/FORS2	600B	3300–6210	780	4 × 1316	1.″3	−20.°0	0.″9	yes
VLT/ISAAC	K_s	32 × 60	0.″7	yes		300V	3400–9500	440	600 + 1200	1.″0	0.°0	1.″5	no
Spitzer/IRAC	3.6 & 5.8 μm	7200				600B	3300–6210	780	5 × 1316	1.″3	33.°5	1.″2	yes
						600B	3300–6210	780	4 × 1316	1.″3	95.°0	1.″3	yes
					VLT/UVES	346 and 580	3030–6840[c]	~40 000	3000	1.″0	0.°0	1.″8	no
						437 and 860	3730–10 600[d]					1.″1	yes
					VLT/X-shooter[e]	UVB	3000–5500	4000	2 × 900	1.″3	43.°7	0.″8	yes
						VIS	5500–10 000	6700	2 × 900	1.″2			
						NIR	10 000–25 000	4000	6 × 300	1.″2			
GRB 050820A: RA = $22^h29^m38^s.114$, Dec = $19°33'36''.61$ (J2000)													
Keck/LRIS	*g*	2620	0.″7	yes	VLT/FORS2	300V			4 × 1316	1.″3	−52.°0	1.″2	yes
HST/ACS	*F625W*	2238				300V	3400–9500	440	8 × 1316	1.″3	34.°0	1.″3	yes
VLT/FORS2	*R*	4 × 500	0.″8	no		300V			4 × 1316	1.″3	83.°0	0.″7	yes
HST/ACS	*F775W*	4404				1028z+OG590			2 × 1316	1.″3	−52.°0	0.″8	yes
HST/ACS	*F850LP*	14 280				1028z+OG590	7730–9480	2560	4 × 1316	1.″3	34.°0	1.″2	yes
Magellan/PANIC	*H*	8460	0.″6			1028z+OG590			2 × 1316	1.″3	83.°0	0.″7	yes
VLT/ISAAC	K_s	32 × 60	0.″7	yes	VLT/UVES	390 and 564	3260–6680[f]	~40 000	1800+1815	1.″0	0.°0	1.″0	yes
Spitzer/IRAC	3.6 & 5.8 μm	3600				437 and 860	3730–10 600[d]		2430				
GRB 050908: RA = $01^h21^m50^s.73$, Dec = $-12°57'17''.30$ (J2000)													
VLT/FORS2	*R*	12 × 500	0.″7	yes	Gemini/GMOS-N	B600+G0305	5118–7882	844	2 × 1200	0.″75	110.°0		
VLT/ISAAC	K_s	32 × 60	0.″6	yes	VLT/FORS1	300V	3400–9500	440	3 × 1200	1.″0	0.°0	0.″6	yes
Spitzer/IRAC	3.6 & 5.8 μm	7200				600B	3300–6210	780	6 × 1345	1.″3	53.°8	1.″2	yes
GRB 070721B: RA = $02^h12^m32^s.95$, Dec = $-02°11'40''.80$ (J2000)													
VLT/FORS2	*R*	24 × 235	0.″5	no	VLT/FORS1	300V	3400–9500	440	5 × 2735	1.″3	−118.°5	1.″2	yes
HST/ACS	*F775W*	6 × 1307			VLT/FORS2	300V	3400–9500	440	4 × 1800	1.″0	−118.°3	1.″2	yes
Magellan/PANIC	*H*	10 320	0.″5										
VLT/ISAAC	K_s	32 × 60	1.″0	yes									

Notes. Co-ordinates were taken from Malesani et al. (in prep.) **Photometry**: observing conditions of Keck and *Magellan* data are quoted from Chen et al. (2009). Column "Photometric?" states if observing conditions were photometric. **Spectroscopy**: observing conditions of the afterglow spectroscopy campaigns, and the VLT/UVES data of GRB 050730 and of GRB 050820A are taken from Fynbo et al. (2009), Ledoux et al. (2009), and Vergani et al. (2009). The VLT/UVES and VLT/X-shooter spectrographs consist of two and three arms, respectively, displayed in the column "Grating". Observations in the different arms are carried out simultaneously. Resolving power of VLT/FORS1+2 and Gemini grisms are given for a slit width of 1″. The stated resolving power of the X-shooter NIR spectrum was decreased during the data reduction to increase S/N. The effective resolving power of the X-shooter NIR arm is around ten times lower. [(a)] Date of observations. GRB 050730: VLT/FORS2 – 2006/03/04 – 05/25, HST/ACS – 2010/06/10, VLT/ISAAC – 2006/03/20, *Spitzer*/IRAC: 2008/03/11; GRB 050820A: Keck/LRIS – July 2006, HST/ACS – *F625W*, *F775W*, *F850LP*: 2005/09/26 and 2006/06/05-11, *Magellan*/PANIC: August 2007, VLT/FORS2 – 2006/05/24, VLT/ISAAC – 2006/05/20, *Spitzer*: 2007/12/23; GRB 050908: VLT/FORS2 – 2007/07/21-08/14, VLT/ISAAC – 2007/07/11, *Spitzer*/IRAC: 2008/08/18; GRB 070721B: VLT/FORS2 – 2007/10/04-11/13, HST/ACS – 2010/11/13, *Magellan*/PANIC – August 2007, VLT/ISAAC – 2007/09/22. [(b)] Date of observations. GRB 050730: VLT/FORS1 600V+GG435 – 2007/02/23-24, VLT/FORS2 600B – PA = 20.°0: 2006/06/22, PA = 0.°0: 2005/07/31, PA = 33.°5: 2006/04/28-05/28, PA = 95.°0: 2006/05/28, VLT/UVES: 2005/07/31, VLT/X-shooter: 2010/04/18; GRB 050820A: VLT/FORS2 300V – PA = −52.°0: 2006/07/22-08/16, PA = 34.°0: 2006/08/31-09/22, PA = 83.°0: 2006/08/17-09/15, 1028z – PA = −52.°0: 2006/08/16, PA = 34.°0: 2006/09/17-22, PA = 83.°0: 2006/08/17, VLT/UVES: 2005/08/20; GRB 050908: Gemini/GMOS-N – 2005/09/08, VLT/FORS1 – 300V: 2005/09/08, 600B: 2007/08/16-09/06; GRB 070721B: VLT/FORS1 – 2007/11/16-12/04, VLT/FORS2 – 2007/07/22. [(c)] Spectral range of the blue and red arms are 3030–3880 Å and 4760–6840 Å, respectively. [(d)] Spectral range of the blue and red arms are 3730–4990 Å and 6600–10 600 Å, respectively. [(e)] The target of the X-shooter observation was QSO J1408-0346. [(f)] Spectral range of the blue and red arms are 3260–4450 Å and 4580–6680 Å, respectively.

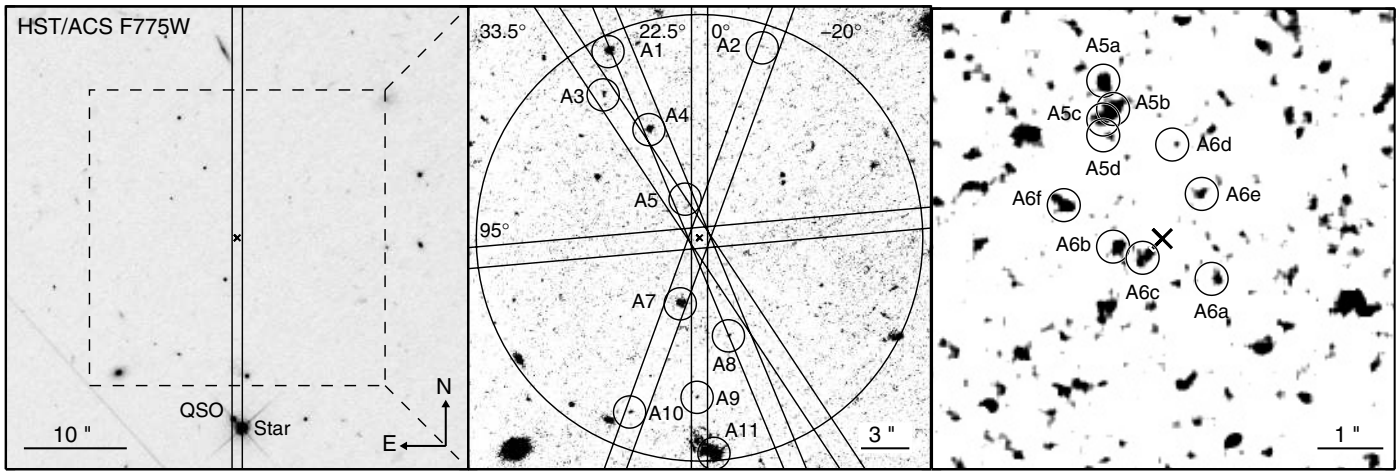

Fig. 1. *Left panel*: the field of view of GRB 050730 ($z = 3.969$) observed in $F775W$ with HST/ACS. *Middle panel*: zoom-in on the inner 28.″8. The different slit orientations from Table 1 are overplotted. *Right panel*: zoom-in on the inner 6″; the panel was smoothed by a boxcar filter (width: 0.″132 = 4 pixel). The afterglow position is marked by an "×" in all panels. The 100-kpc radius (shown in the middle panel) represents the assumed maximum impact parameter of the absorber at $z = 3.56$. Objects are labelled if they lie within the circle and if they are covered by any of the slits. Their magnitudes are summarised in Table 4.

pixel scale of these drizzled images is 0.″05 in contrast to that of the images of GRBs 050730 and 070721B.

Spitzer data – GRBs 050730, 050820A, and 050908 were observed with the Infrared Array Camera aboard *Spitzer* (IRAC; Fazio et al. 2004) in the bandpasses centred at 3.6 and 5.8 μm. We downloaded the processed PBCD data from the *Spitzer* Heritage Archive and followed the basic procedures for aperture photometry in the IRAC instrument handbook[3], using an extraction radius of two native pixels (2.″4, or four pixels in the default archive resampling).

Photometry – To measure the total flux, we applied aperture photometry, using Source Extractor (Bertin & Arnouts 1996), and applied an aperture correction assuming a stellar point-spread function (PSF; for the aperture correction of the HST images see Sirianni et al. 2005).

The quasar in the field of GRB 050730 is strongly blended with a foreground star at a projected distance of 1.″2. To perform reliable photometry, the contaminating star was subtracted from the VLT/FORS1 images. A model of the FORS1 PSF was constructed from ∼60 field stars using Daophot as implemented in `IRAF`. This PSF model was then fitted simultaneously to the star and the QSO. To test the quality of the fit, we subsequently subtracted the stellar contribution from the input image. Photometry was then performed in the final star-subtracted image.

Instrumental magnitudes obtained from optical ground-based data were calibrated against 2–3 photometric standard stars (Landolt 1992; Stetson 2000). NIR magnitudes were calibrated with more than three 2MASS stars and HST magnitudes against zeropoints, computed from their FITS headers.

2.2.2. Spectroscopy

VLT/FORS1 and FORS2, Gemini/GMOS and VLT/UVES data – FORS and Gemini data were reduced in a standard way with `IRAF` (for more details see Fynbo et al. 2009). The data reduction of the UVES data is described in Ledoux et al. (2009).

VLT/X-shooter data – The QSO in the field of GRB 050730 was observed with X-shooter. These data were reduced with the X-shooter pipeline v1.2.2[4]. The one-dimensional spectrum of the QSO ($R = 20.76$ mag; corrected for Galactic extinction) in the field of GRB 050730 could not be extracted with the X-shooter pipeline, because it is blended with the 18.2-mag-bright foreground star 1.″2 SW mentioned above (see Fig. 1).

To estimate the flux of the quasar over the entire wavelength range of the X-shooter spectrograph, we proceeded in the following way. For each arm, we first extracted a profile of the superposed spectral PSFs at several wavelengths. Each profile was best described by two Gaussians, representing the QSO and the star. The centre of their peaks and the widths did not change with wavelength, allowing us to fix these parameters to their mean values for each arm of the X-shooter spectrograph. Then, we extracted the profile for every wavelength and fitted it with the aforementioned model, using the routine `mpfit` by Markwardt (2009), in `IDL`. To identify outliers, a nine-point median profile was fitted for every wavelength, i.e. four points redward and four points blueward of the considered wavelength. Data points were rejected if they deviated by more than 3σ from the median spectral PSF of the quasar and the star.

The QSO was barely visible in the NIR spectrum. We therefore determined the centre of peak and the FWHM of the star and set the QSO centre of peak to its expected position. Furthermore, we reduced the spectral resolution to increase the signal-to-noise ratio (S/N) by rebinning the spectrum. The uncertainties in the FWHMs and the centre of peaks varied between 0.06 and 0.39 px and 0.3 and 0.18 px for each arm (pixel scale: UVB and VIS 0.″16/px, NIR 0.″21/px), respectively, small enough to be neglected.

We compared the quality of our method with the MCS deconvolution technique developed by Magain, Courbin, & Sohy (Magain et al. 1998) used in Letawe et al. (2008; see also Courbin et al. 2000). This method requires an unblended star to be observed with the identical instrument setup. Because of

[3] http://sha.ipac.caltech.edu/applications/Spitzer/SHA/

[4] http://www.eso.org/sci/software/pipelines/

Table 2. Properties of the intervening sub-DLAs and DLAs.

GRB	z_{GRB}	z_{abs}	log N(H I)	[Si/H]	EW_{rest} (Si II λ1526) (Å)	Detected lines	References
050730	3.969	3.56439	20.3 ± 0.1	<–1.3	<1.01[a]	Al II, Fe II, Si II, Si II*, C IV, Si IV	1, 2, 3
		3.02209	19.9 ± 0.1	–1.5 ± 0.2[b]	...	Al II, Fe II, Si II	
050820A	2.615	2.3598[c]	20.1 ± 0.2	–1.5 ± 0.2	0.17 ± 0.01[d]	Fe II, Si II, C IV, Mg II	4
050908	3.3467	2.6208	20.8 ± 0.1[d,e]	>–1.40[d]	2.24 ± 0.06	Al II, Fe II, Si II, C IV	2
070721B	3.6298	3.0939[g]	20.1 ± 0.3[d,e]	>–0.66[d]	2.35 ± 0.69[d]	Al II, Fe II, Si II, C IV	2

Notes. [(a)] This line is blended. The EW listed is the value of the blend. [(b)] Without ionisation correction. [(c)] Vergani et al. (2009) reported EW_{rest} (Mg II λ2796) < 0.42 Å with a most likely value of 0.31 Å. [(d)] This work. [(e)] Fynbo et al. (2009) suggested that the absorber is a sub-DLA. [(f)] Derived in the optically thin limit. [(g)] Chen et al. (2009) and Fynbo et al. (2009) proposed that a galaxy 0.″9 SE of the afterglow position is the galaxy counterpart to the intervening absorber.

References. (1) Chen et al. (2005); (2) Fynbo et al. (2009); (3) Starling et al. (2005); (4) Vergani et al. (2009).

Table 3. Properties of selected Mg II absorbers.

GRB	z_{GRB}	z_{abs}	EW_{rest} (Mg II λ2796) (Å)	Detected lines	References
050730	3.969	2.25313	<0.78 (0.65)[†]	Fe II, Mg I, Mg II	1, 2
		1.7731[a]	0.93 ± 0.03[†]	Fe II, Mg I, Mg II	1, 2
050820A	2.6147	1.4288	1.32 ± 0.02	Fe II, Mg I, Mg II	1
		0.6915	2.87 ± 0.01[†]	Ca II, Fe II, Mg II	1
050908	3.3467	1.5481	0.82 ± 0.07[†]	Fe II, Mg II	3

Notes. We only summarise the properties of those Mg II absorbers that most likely have an intervening sub-DLA or DLA. Following the typical approach in the literature, we call absorbers with EW_{rest} (Mg II λ2796) > 1.0 Å strong, with 0.3 Å < EW_{rest} (Mg II λ2796) < 1.0 Å intermediate and with EW_{rest} (Mg II λ2796) < 0.3 Å weak systems. Absorbers are marked by [†] if the doublet is saturated. [(a)] Chen et al. (2005) identified two velocity components that are separated by 57 km s^{-1}.

References. (1) Vergani et al. (2009); (2) Prochaska et al. (2007a); (3) Fynbo et al. (2009).

the short slit length, no such object was covered by the slit. For a rough estimate, we used the observed standard star as reference, although it was observed with a slit width of 5″. Within the errors both methods give the same results.

To flux-calibrate the spectrum, we reduced the data of the standard star GD50 with the X-shooter pipeline. The 1D spectrum was extracted using the routine `apall` in optimal extraction mode. The spectrum was then divided by the corresponding reference spectrum from the `CALSPEC HST` database (Bohlin & Gilliland 2004) to deduce the response function. In addition, we corrected the flux-calibrated standard star spectrum for undulations by smoothing the ratio between the observed flux-calibrated and expected spectra with a Hamming filter (window size: 40 Å in the UVB and VIS arm) in regions that were not affected by strong telluric lines or stellar absorption features. We then applied the corrected response function to the QSO and used the acquisition image to secure the absolute flux calibration. Finally, we followed Cardelli et al. (1989) to correct the QSO for Galactic dust attenuation ($E(B-V) = 0.048$ mag). No attempt was made to correct for telluric absorption lines due to the lack of a suitable telluric standard star observed the same night. This has no implications on our analysis.

2.3. SED fitting

The photometric SEDs of the galaxies were modelled within `Le Phare` (Arnouts et al. 1999; Ilbert et al. 2006)[5]. Here, we used a grid of galaxy templates based on the Bruzual & Charlot (2003) stellar population synthesis models with a Chabrier IMF (Chabrier et al. 2000) and a Calzetti (Calzetti et al. 2000) dust attenuation curve. If prior information about the redshift was available from spectroscopy, we fixed this parameter to the respective value. For a description of the galaxy templates, physical parameters of the galaxy fitting and their error estimation we refer to Krühler et al. (2011). To account for zeropoint offsets in the cross calibration and absolute flux scale, an systematic error contribution of 0.05 mag was added in quadrature to the uncertainty introduced by photon noise.

3. Results

Afterglow spectroscopy allowed us to identify seven intervening sub-DLAs and DLAs in six GRB fields. For four of these fields, we had sufficient data to elucidate the nature of several galaxy counterpart candidates. In the following, we describe how we selected the candidates, and present the properties of the intervening sub-DLAs and DLAs towards GRBs 050730, 050820A, 050908 and 070721B and our findings on the most likely galaxy counterpart for each field. A summary of the properties of the intervening sub-DLAs and DLAs is presented in Tables 2 and 3. Most of the values are taken from the literature.

To select candidates that are close enough to the GRB line of sight to produce an intervening absorption-line system in the afterglow spectrum, we had to set an upper limit on the extent of the possible DLA galaxies. Theoretically, it is very difficult to set a meaningful upper boundary, because different models exist for

[5] http://www.cfht.hawaii.edu/~arnouts/LEPHARE

their galaxy counterparts. The observed impact parameter distribution of confirmed DLA galaxies, based on Péroux et al. (2011) and Krogager et al. (2012), extends from 0.4 to 182 kpc and has a mean value of ∼25 kpc. The impact parameter distribution of DLA galaxy candidates by Rao et al. (2011) shows similar characteristics. The majority of DLA galaxies have a small impact parameter, but there are few cases with large impact parameters (∼100 kpc). We therefore followed the statistical approach by Rao et al. (2011), who used the galaxy number density as a function of impact parameter as a criterion. They found that the galaxy number density is comparable to the number density of foreground and background galaxies, i.e. a chance association is more likely if the impact parameter exceeds 100 kpc. As a first assumption, we limited our study to those candidates within 100 kpc from the GRB line of sight, keeping in mind that this value was derived for intervening DLAs between $z = 0.5$ and 0.8.

3.1. GRB 050730

GRB 050730 occurred at a redshift of $z = 3.969$. Its afterglow spectrum contains an intervening sub-DLA ($\log N(\mathrm{H\,I}) = 19.9 \pm 0.1$, $[\mathrm{Si/H}] = -1.5 \pm 0.2$)[6], and an intervening DLA ($\log N(\mathrm{H\,I}) = 20.3 \pm 0.1$, $[\mathrm{Si/H}] < -1.3$) at $z = 3.02209$ and $z = 3.56439$, respectively (Tables 2, 3). In addition, the afterglow light traversed an intermediate and a strong Mg II absorber at $z = 2.25313$ and 1.7731, respectively.

In Fig. 1, we show the field of GRB 050730 and zoom-ins on the inner 28.″8 and 6.″0; the region at which the impact parameter exceeds 100 kpc is highlighted. At the redshift of the aforementioned absorption-line systems, the maximum impact parameter of 100 kpc translates into a transverse distance between 12.″1 and 13.″9; the lower value belongs to $z = 1.7731$ and the higher to $z = 3.56439$, including the astrometric uncertainty of the afterglow localisation of 0.″3.

The GRB was the target of an extensive spectroscopic campaign; several low-resolution spectra with a total of five different position angles (PA) were obtained with VLT/FORS1 and VLT/FORS2 (Fig. 1, Table 1). Within the 100-kpc radius, 19 objects were covered by a slit. In Table 4 we summarise their magnitudes in different filters and their angular distances from the afterglow position. Four of these objects were bright enough to allow the extraction of a spectrum. The VLT/FORS1 spectra of objects A1 and A4 are of very low S/N. We detect their continua down to 4500 Å, but we detect no absorption or emission lines. If these objects were the galaxy counterparts to the sub-DLA and DLA, we would expect to see the onset of the Lyα forest at ∼4890 Å and ∼5549 Å, respectively, which we do not observe. The Lyα non-detection and the extension of the continuum to even shorter wavelengths, excludes them from being the galaxy counterparts. We detect the continuum of object A7 at very low S/N in the VLT/FORS2 data, but no absorption or emission lines. The objects A1, A4 and A7 are likely late-type stars based on their colours and the fact that the morphology and size of their PSFs ($FWHM = 0.″11$) do not differ from point sources. Object A11 lies at the edge of the 100-kpc radius. We detect its continuum down to 4630 Å in the VLT/FORS2 data and a drop in flux blueward of it. Assuming that this is the Balmer break, the redshift of the galaxy is ∼0.16, which disagrees with that of the intervening absorbers.

In conclusion, we identified no galaxy counterpart candidate of the intervening sub-DLA and DLA down to a limiting magnitude of $F775W = 25.7\,(24.6)$ mag and of any of the intermediate Mg II absorbers down to a limiting magnitude of $F775W = 26.5\,(25.1)$ mag, assuming a maximum impact parameter 50 (100) kpc. These limits were calculated by considering all objects within 50 (100) kpc but excluding those for which we elucidated the nature or those with a stellar PSF.

Fynbo et al. (2009) reported the serendipitous discovery of a QSO at the redshift of $z = 3.023$, very similar to the redshift of the sub-DLA in the afterglow spectrum. The QSO is 17.″5 south of the afterglow position (see Fig. 1, Table 4), corresponding to a projected distance of 136.7 kpc at $z = 3.02209$, the redshift of the sub-DLA towards the GRB. It has a brightness of 20.76 ± 0.05 mag in the R-band (corrected for Galactic extinction, Table 4), but is blended with a 18.2-mag bright K-type star. Strictly speaking, the impact parameter exceeds the assumed maximum impact parameter of 100 kpc. Given the redshift coincidence with the sub-DLA in the afterglow spectrum, we discuss this correlated structure in Sect. 4.4.

3.2. GRB 050820A

Ledoux et al. (2005) and Vergani et al. (2009) reported an intervening sub-DLA at $z = 2.3598$ with $\log N(\mathrm{H\,I}) = 20.1 \pm 0.2$ and a metallicity of $[\mathrm{Si/H}] = -1.5 \pm 0.2$ and two strong Mg II absorbers between $z = 0.6915$ and 1.6204 towards GRB 050820A ($z_{\mathrm{GRB}} = 2.615$, Tables 2, 3).

In Fig. 2, we show the inner 29″ around the afterglow position and highlight the region at which the impact parameter is 100 kpc. At the redshift of the intervening absorbers, the maximum impact parameters correspond to 12.″4 for $z = 2.3598$ and 14.″4 for $z = 0.6915$, including the uncertainty of 0.″4 in the afterglow localisation.

After the afterglow faded, several spectra were acquired with VLT/FORS2. In addition, the field was also the target of an extensive photometric campaign covering nine filters from 473.1 nm (g'-band) to 5.8 μm; for full details we refer to Sect. 2.1 and Table 1. This allows us to elucidate the nature of several objects within 100 kpc, not only of those that were covered by a slit and bright enough for a spectrum to be extracted. In the following, we only consider those objects that are either detected in at least five filters to attempt SED modelling, or fall in one of the slit positions. In total, 11 objects within 100 kpc of the afterglow position fulfil these criteria (Fig. 2, Table 4). Among them, nine fell into one of the slits.

The two brightest objects (B4 and B10) within the 100 kpc radius are late-type stars. The spectrum of B9 exhibits two emission lines at 5322.1 and 7149.3 Å both detected at ∼6σ confidence level (Fig. A.1). We identify these lines as [O II] λ3727 and [O III] λ5007 at a common redshift of $z = 0.428$.

The spectrum of object B2 (Fig. A.2) has a continuum break at ∼6750 Å and absorption lines at 6660.2 and 6719.5 Å. These features are consistent with the Balmer break and Ca II K&H absorption at a redshift of $z = 0.693$. The S/N of the VLT/FORS2 spectra of B3 and B6 are too low for redshift determination[7]. Both objects are detected in the nine filters, see Figs. A.3 and A.5. The best fits to their SEDs suggest that B3 and B6 are galaxies at $z = 0.67^{+0.05}_{-0.06}$ and $1.46^{+0.07}_{-0.41}$, respectively. Object B5 was detected in five filters from 473 to 766 nm (Fig. A.4). The

[6] The metallicity is not corrected for ionisation effects.

[7] The spectrum of B3 shows a prominent emission line at ∼6310 Å. The bright [O I] sky emission line at 6300.3 Å partly overlaps with this feature, making the identification ambiguous. If this is indeed an emission line of galaxy B3, it is likely [O II] λ3727 redshifted to $z \sim 0.693$, coinciding in redshift with a strong Mg II absorber.

Table 4. Galaxy counterpart candidates of the intervening absorption line systems.

GRB 050730 (GRB: $z = 3.969$, DLA: $z = 3.56439$, sub-DLA: $z = 3.02209$, Mg II absorbers: $z = 2.25313, 1.7731$)											
Candidate	Remark	θ ($''$)	R (mag)	$F775W$ (mag)	K_s (mag)	3.6 μm (mag)	5.8 μm (mag)				
A1	star	12.8	23.46 ± 0.03	23.08 ± 0.01	22.51 ± 0.25	23.30 ± 0.20					
A2		12.3		28.50 ± 0.26							
A3		10.6	26.53 ± 0.12	26.60 ± 0.09							
A4	star	7.3	23.88 ± 0.03	23.71 ± 0.02							
A5a		2.5	27.20 ± 0.27	27.98 ± 0.18							
A5b[a]		2.1		28.16 ± 0.19							
A5c[a]		2.0		28.43 ± 0.22							
A5d		1.8		28.84 ± 0.30							
A6a		1.0		28.64 ± 0.26							
A6b		0.7		28.37 ± 0.24							
A6c		0.4		28.11 ± 0.19							
A6d		1.4		28.64 ± 0.26							
A6e		0.9		28.64 ± 0.26							
A6f		1.5		28.29 ± 0.20							
A7	star	4.2	23.38 ± 0.03	22.84 ± 0.01	22.28 ± 0.15	22.78 ± 0.15					
A8		6.3		27.49 ± 0.12							
A9		9.8		27.38 ± 0.12							
A10		11.5		27.10 ± 0.13							
A11[b]	$z \sim 0.16?; z < 2.81$	13.3									
QSO[c]	$z = 3.022$	17.5	20.87 ± 0.05	~20.58							
Star[c]	star	18.3	18.20 ± 0.04								
GRB 050820A (GRB: $z = 2.615$, DLA: $z = 2.3598$, Mg II absorbers: $z = 1.4288, 0.6915$)											
Candidate	Remark	θ ($''$)	g (mag)	$F625W$ (mag)	R (mag)	$F775W$ (mag)	$F850LP$ (mag)	H (mag)	K_s (mag)	3.6 μm (mag)	5.8 μm (mag)
B1[d]		11.8		25.18 ± 0.04		24.87 ± 0.03	24.90 ± 0.06			23.45 ± 0.30	
B2	$z = 0.693$	12.3	25.41 ± 0.07	23.59 ± 0.03	23.20 ± 0.03	22.35 ± 0.01	21.81 ± 0.05	20.81 ± 0.10	20.47 ± 0.05	20.59 ± 0.05	21.40 ± 0.20
B3	$z = 0.67^{+0.02}_{-0.07}$	5.2	25.24 ± 0.06	23.90 ± 0.04	23.65 ± 0.04	23.01 ± 0.02	22.57 ± 0.05	21.41 ± 0.14	21.05 ± 0.07	20.94 ± 0.06	21.04 ± 0.18
B4	star	2.8	23.39 ± 0.05	22.11 ± 0.01	21.97 ± 0.03	21.68 ± 0.01	21.34 ± 0.01	20.94 ± 0.11	21.19 ± 0.07	21.65 ± 0.10	21.68 ± 0.32
B5	$z = 0.9 \pm 0.1$	3.7	26.68 ± 0.14	26.36 ± 0.09	26.48 ± 0.26	25.58 ± 0.06	25.36 ± 0.06				
B6	$z = 1.5^{+0.2}_{-0.3}$	4.9	25.23 ± 0.06	24.94 ± 0.09	24.80 ± 0.09	24.32 ± 0.04	23.67 ± 0.05	22.28 ± 0.21	22.20 ± 0.15	21.81 ± 0.10	
B7[a]	$z = 2.615$	1.6	25.75 ± 0.08	25.99 ± 0.07	25.66 ± 0.10	25.90 ± 0.06	25.83 ± 0.08				
B8N[a]	$z = 2.615$	0.3		26.16 ± 0.08		25.83 ± 0.08	26.18 ± 0.06				
B8S[a]		0.1		26.19 ± 0.08		25.72 ± 0.07	25.82 ± 0.05				
B9	$z = 0.428$	3.4	25.49 ± 0.07	24.94 ± 0.05	24.45 ± 0.07	24.76 ± 0.03	24.57 ± 0.04				
B10	star	3.6	22.11 ± 0.05	20.58 ± 0.00	20.31 ± 0.03	19.69 ± 0.00	19.16 ± 0.00	18.60 ± 0.05	18.81 ± 0.04	19.51 ± 0.03	20.29 ± 0.09

Notes. Observed magnitudes are given in the AB system (not corrected for Galactic extinction). VLT and *Magellan* Vega-magnitudes were converted into the AB system by adding VLT/R 0.21 mag (Blanton & Roweis 2007), VLT/K_s 1.895 mag (ESO), and *Magellan*/H 1.34 mag. Selective Galactic extinctions, $E(B-V)$, are 0.051 and 0.044 mag, for GRBs 050730 and 050820A, respectively. Impact parameters were derived from the HST images, if available, otherwise from R-band images. The uncertainty in the impact parameter is $0\farcs3$–$0\farcs4$. Spectra were extracted for boldfaced objects. Based on the spectrum, the SED or the shape and colour of an object, we report in the column "remark" if it is a star or at which redshift the galaxy is. The 3σ limiting magnitudes are GRB 050730: $R = 27.1$, $F775W = 28.6$, $K_s = 22.8$, 3.6 μm = 23.5, 5.8 μm = 21.5 mag, GRB 050820A: $g' = 27.6$, $F625W = 27.8$, $R = 26.1$, $F775W = 28.1$, $F850LP = 28.0$, $H = 23.0$, $K_s = 23.0$, 3.6 μm = 23.5, 5.8 μm = 21.7 mag. [(a)] Blended object. The magnitude is only an estimate. The spectrum can be the integrated spectrum of the blended objects. [(b)] The object consists of at least two galaxies and is detected in all filters. We do not report any magnitude of the individual objects or the compound in this work. We detect the continuum down to 4630 Å. If this break is caused by Lyα absorption, the redshift is $z = 2.81$; alternatively if this is the redshifted 4000 Å feature, the redshift is $z = 0.16$. [(c)] The R-band brightness of the quasar and the star were obtained from an afterglow image taken on 23 February 2007 using PSF photometry (Sect. 2.2.1). The blended star is saturated in the HST image. The PSF was subtracted with the tool Tiny Tim (Krist 1993) assuming a *FWHM* of $5''$. While the wings of the star were partly removed, the residuals in the core are quite strong. The measurement of the QSO magnitude is only an estimate. [(d)] The compound is a blend of several individual objects. We only report the brightness in the HST images of the brightest object.

Table 4. continued.

GRB 050908 (DLA: $z = 3.3467$, DLA: $z = 2.6208$, Mg II absorber: $z = 1.5481$)						
Candidate	Remark	θ ($''$)	R (mag)	K_s (mag)	3.6 μm (mag)	5.8 μm (mag)
C1	$z \approx 2.71$	12.6	27.10 ± 0.20			
C2		11.5	24.96 ± 0.04		23.25 ± 0.19	
C3		6.6	25.97 ± 0.09			
C4[a]		12.4	26.17 ± 0.09			
C5[a,b]		3.7	25.05 ± 0.04		23.65 ± 0.23	22.44 ± 0.44
C6[a,b]		2.8	25.39 ± 0.05			
C7[b]		1.1	26.98 ± 0.18			
C8		5.5	26.59 ± 0.21			
C9		2.5	25.96 ± 0.12		~25.0 ± 0.5	
GRB 070721B (GRB: $z = 3.6298$, DLA: $z = 3.0939$)						
Candidate	Remark	θ ($''$)	R (mag)	$F775W$ (mag)	H (mag)	K_s (mag)
D1		12.8		27.40 ± 0.12		
D2a[a]	$z \approx 2.64$	3.0		27.34 ± 0.12		
D2b[a]		2.8		28.23 ± 0.22		
D3	$z = 3.096$	1.0	24.48 ± 0.02	24.41 ± 0.02	23.40 ± 0.07	23.56 ± 0.23
D4	$z = 3.631$	0.1		27.31 ± 0.15		
D5		6.9	26.82 ± 0.18	26.44 ± 0.10		
D6a[a]	$z \approx 2.64$	11.7		25.05 ± 0.04		
D6b[a]		12.2		26.90 ± 0.09		
D7	$z = 3.615$	20.7	23.77 ± 0.01	23.74 ± 0.03	24.02 ± 0.11	23.20 ± 0.17

Notes. Selective Galactic extinctions, $E(B-V)$, are 0.025 and 0.031 mag for GRBs 050908 and 070721B, respectively. Spectra were extracted for boldfaced objects. Based on the spectrum or the SED of an object, we show in the column "remark" if it is a star or at which redshift the galaxy is. The 3σ limiting magnitudes are GRB 050908: $R = 27.4$, $K_s = 23.0$, 3.6 μm = 23.8, 5.8 μm = 22.3 mag and GRB 070721B: $R = 27.5$, $F775W = 28.7$, $H = 23.1$, $K_s = 23.2$ mag. [(a)] Blended object. The magnitude is only an estimate. The spectrum is the integrated spectrum of the blended objects. [(b)] We did not attempt photometry on objects that are strongly blended in the *Spitzer* data in this work, with the exception of objects C5, C6, and C7, which are sufficiently closely blended that we report the (summed) photometry of all three objects as a group.

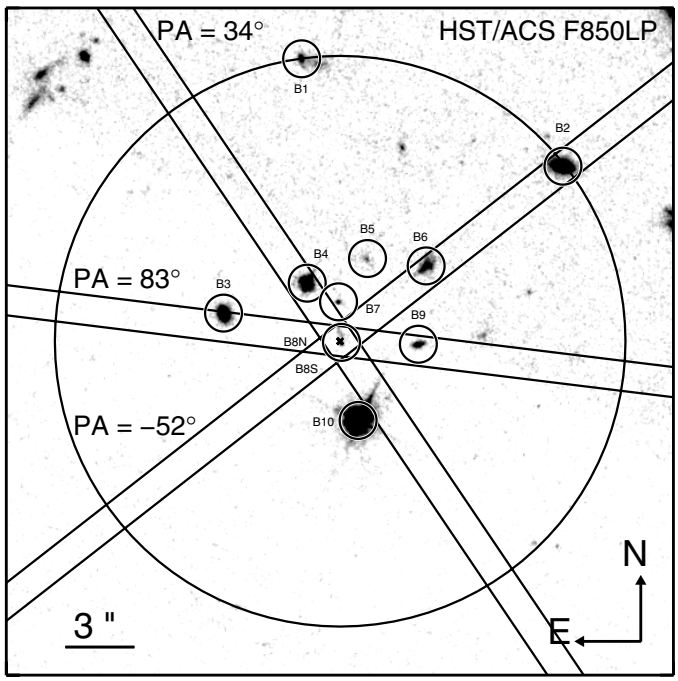

Fig. 2. Similar to Fig. 1, but for GRB 050820A ($z = 2.615$). In contrast to GRB 050730, the field of GRB 050820A was observed in nine filters ranging from 473 nm to 5800 nm, in addition to extensive spectroscopy campaigns. This allowed us to construct the SED of several objects in the field of view. The width of the displayed field is 29″, twice the maximum impact parameter of 100 kpc of the strong Mg II absorber at $z = 0.6915$, while the circle displays the maximum impact parameter of 100 kpc at the redshift of the intervening sub-DLA at $z = 2.3598$. Every object within 100 kpc is labelled if it is either detected in at least five filters or covered by a slit. Objects B7 and B10 appear to be not in the slit, due to the smaller PSF of the HST in comparison to the VLT.

SED is best described by a young and small galaxy at $z = 0.9^{+0.1}_{-0.2}$. We caution that the solution is not unique because the galaxy is only detected in five filters. The redshifts of B2, B3, B5 and B6 match the redshifts of the strong Mg II absorbers at $z = 0.6915$ and 1.4288 towards GRB 050820A, see Table 3.

The continua of objects B7 and B8 are visible in the 2D spectrum. Because of the seeing, the spectrum of B8 is not resolved into the two objects B8N and B8S as seen in the HST image. The extracted 1D spectra of B7 and B8 have a low S/N and thus their redshifts cannot be determined. Recently, Chen (2012) observed the field with the IR echellette spectrograph FIRE mounted on the *Magellan* telescope. The slit was oriented to cover object B7 and the compound B8. Based on these observations, Chen (2012) found that the galaxy B7 and the host complex B8 are a group of galaxies at $z \simeq 2.613$, in contrast to Chen et al. (2009), who suggested that B7 and B8S are interacting galaxies forming the strong Mg II absorber at $z = 0.692$.

Although we elucidated the nature of all objects within 3.″7 that are visible in the HST images, we did not identify a possible galaxy counterpart of the intervening sub-DLA. We also did not find any candidate brighter than $F625W = 26.7$ (26.6) mag with an maximum impact parameter of 50 (100) kpc.

3.3. GRB 050908

The afterglow spectrum of GRB 050908 ($z = 3.3467$), obtained with VLT/FORS1, revealed an intervening DLA at $z = 2.6208$ with $\log N(\mathrm{H\,I}) = 20.8 \pm 0.1$, as derived from the Voigt profile fit shown in Fig. 3. We thus revise the conclusion by Fynbo et al. (2009) that this intervening absorber is a sub-DLA. This DLA is peculiar for its strong metal lines ($EW_{\rm rest}$ (Si II λ1526) = 2.24 ± 0.06 Å) that are stronger than those of most intervening DLAs (Fynbo et al. 2009, their Fig. 11). In addition, the

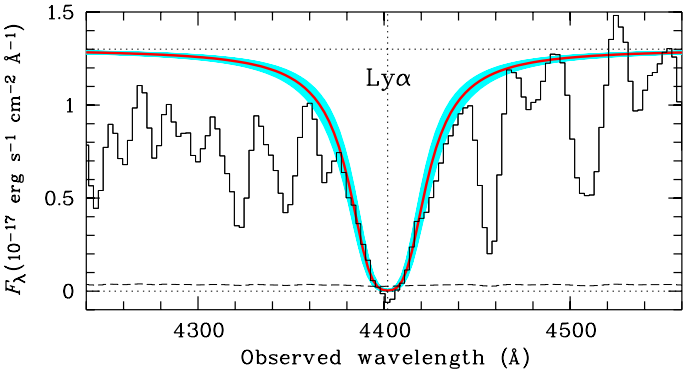

Fig. 3. GRB 050908 afterglow spectrum obtained with VLT/FORS1, centred on the intervening Lyα absorption line ($z_{\rm DLA}$ = 2.6208; $\log N$(H I) = 20.8 ± 0.1). A neutral hydrogen column density fit to the damped Lyα line is shown with a solid line, while the shaded region indicates the 1σ errors.

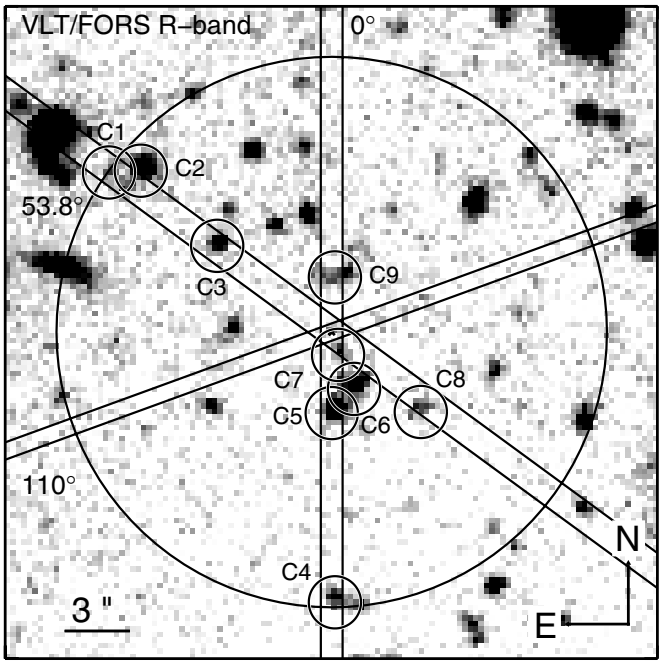

Fig. 4. Similar to Fig. 1, but for GRB 050908 (z = 3.3467). The different slit orientations from Table 1 are overplotted. The circle radius of 12.″7 represents the assumed maximum impact parameter of 100 kpc of the intervening sub-DLA at z = 2.6208. Objects are labelled if they lie within the circle and if they are covered by any of the slits. Their magnitudes are summarised in Table 4.

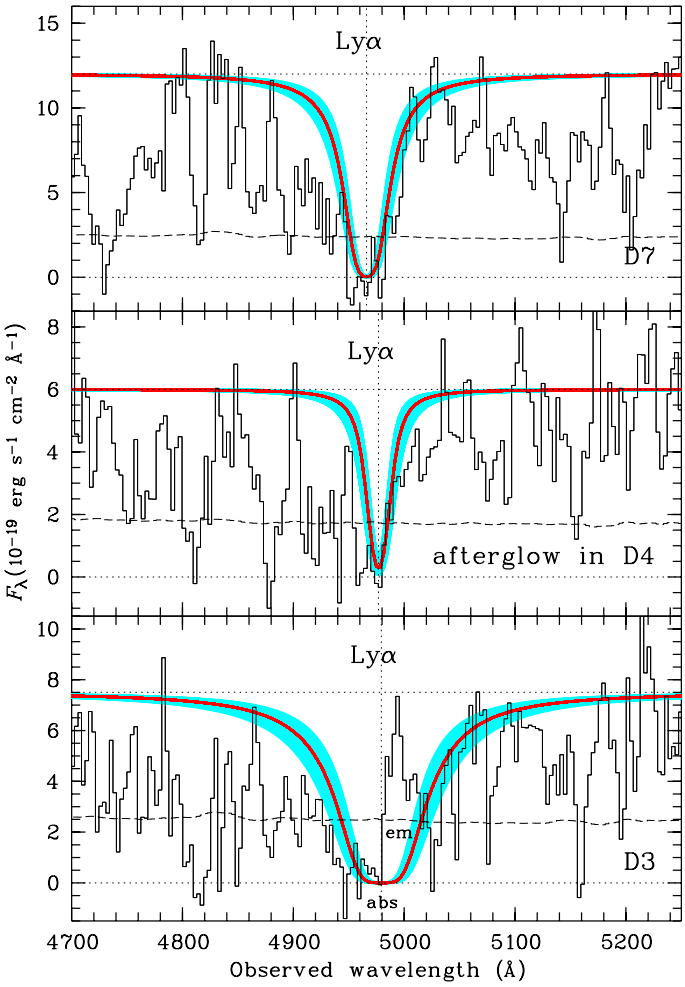

Fig. 5. Fit of the intervening Lyα absorption features towards galaxy D7 ($z_{\rm abs}$ = 3.085; $\log N$(H I) = 20.7 ± 0.2) and towards GRB 070721B ($z_{\rm abs}$ = 3.0939; $\log N$(H I) = 20.1 ± 0.3), and the Lyα absorption feature in the DLA galaxy D3 ($z_{\rm abs}$ = 3.096; $\log N$(H I) = 21.3 ± 0.2). The fit of D3 nicely shows the Lyα emission in the red part of the trough. The afterglow spectrum (D4) was acquired with VLT/FORS2, while the displayed spectra of D3 and D7 were extracted from the VLT/FORS1 data. The fit is shown with a solid line, while 1σ errors are displayed with the shaded region.

afterglow spectrum consists of an intermediate Mg II absorber at z = 1.5481. The properties of both absorbers are summarised in Tables 2 and 3.

At the redshift of the intervening Mg II absorber and the DLA, an impact parameter of 100 kpc corresponds to an angular distance of 12.″0 and 12.″6, respectively, including the uncertainty in the afterglow position of 0.″3. The GRB field and the galaxies within this impact parameter are shown in Fig. 4.

An afterglow spectrum was acquired with VLT/FORS1 (PA = 0.°0) and with Gemini-N/GMOS (PA = 110.°0). In addition, another spectrum was obtained with VLT/FORS1 (PA = 53.°8) two years later (Table 1). Both FORS1 spectra cover several faint objects (R ∼ 26 mag) within the 100-kpc radius (Fig. 4, Table 4). Apart from the afterglow, we only detect a very weak emission feature at ∼4512 Å at the position of C1. Assuming that this is a genuine emission line, the line is likely Lyα redshifted to z ∼ 2.71, and not [O II] because of the non-detection of Hβ and [O III] λ5007. The Gemini spectrum (PA = 110.°0) does not cover any of the faint objects visible in the R-band image and we do not detect any emission line in these data.

Since the field is quite crowded and the amount of spectroscopic and multi-filter data are limited, we can only place a shallow upper limit on the brightness of the galaxy counterpart of the two absorption-line systems. Assuming a maximum impact parameter of 50 or 100 kpc, the galaxy counterpart cannot be brighter than 25 mag and 24.7 mag in the R band.

3.4. GRB 070721B

The VLT/FORS2 afterglow spectrum of GRB 070721B (z = 3.6298) revealed an intervening absorber at z = 3.0939, a sub-DLA with strong metal absorption lines ($EW_{\rm rest}$ (Si II λ1526) = 1.71 ± 0.54 Å; Table 2). Figure 5 displays the Lyα absorption profile; the Voigt profile fit gives $\log N$ (H I) = 20.1 ± 0.3. In

Fig. 6 we show the field of view and highlight the maximum impact parameter of 100 kpc, corresponding to 13.″3 at $z = 3.09$, including the uncertainty in the afterglow localisation of 0.″4.

Four months after the GRB, an additional spectrum with PA $= -118.^{\circ}5$ was acquired with VLT/FORS1. The spectrum covers several objects within the 100 kpc radius (Table 4). The 2D spectrum shown in Fig. 7 reveals that this is a very complex and perplexing line-of-sight. The galaxy D7, which was also detected in the 2D-spectrum of the afterglow, is a bright Lyα emitter at $z = 3.615$ – very similar to the redshift of the GRB. Object D4 is the host galaxy of GRB 070721B and is only detected by its Lyα emission line in the 2D spectrum (Fig. 7). The emission line redshift ($z_{\rm em} = 3.631$) differs slightly from the absorption-line redshift ($z_{\rm abs} = 3.6298$), derived from metal lines in the afterglow spectrum (see Milvang-Jensen et al. 2012, for a detailed discussion). In the spectrum of galaxy D3 we detect several strong metal lines as well as a strong Lyα absorption line at a common redshift of $z = 3.096$. This galaxy has an impact parameter of only 1″ relative to the GRB position. Hence, D3 must be the galaxy counterpart of the DLA seen in the GRB afterglow spectrum. This was also suggested by Fynbo et al. (2009) and Chen et al. (2009). Intriguingly, D7 also has an intervening strong Lyα absorption line at a very similar redshift ($z = 3.085$); we derive a H I column density of 20.7 ± 0.2 from the Voigt profile fitting, as shown in Fig. 5[8]. However, we do not detect metal lines associated with this intervening absorption line system[9]. At that redshift the angular separation between D3 and D7 of 20.″7 translates into a transverse distance of 161 kpc. The weak trace below D7 is from the galaxy D6. This spectrum displays a single strong emission line. It is very likely Lyα at $z_{\rm em} = 2.642$ and not [O II λ3727], because of the lack of Hβ and [O III] λ5007 in emission. The spectrum of D2 shows that this is also a Lyα emitter at a very similar redshift to that of D6, $z_{\rm em} \simeq 2.644$. In the spectrum of the afterglow we detect absorption lines from Lyα, C II λ1334 and the C IV doublet (unresolved) at $z_{\rm abs} = 2.655$ albeit a low S/N. The velocity distance between the absorption and emission line redshifts is ~900 km s^{-1}.

The region around Lyα in the spectrum of D3 seems to be a superposition of an emission line on top of a broad absorption line (see Figs. 5, 7). Such a feature has been observed in several high-z galaxies (e.g. Pettini et al. 1998a,b, 2000). We estimate an H I column density of $\log N$(H I) $= 21.3 \pm 0.2$.

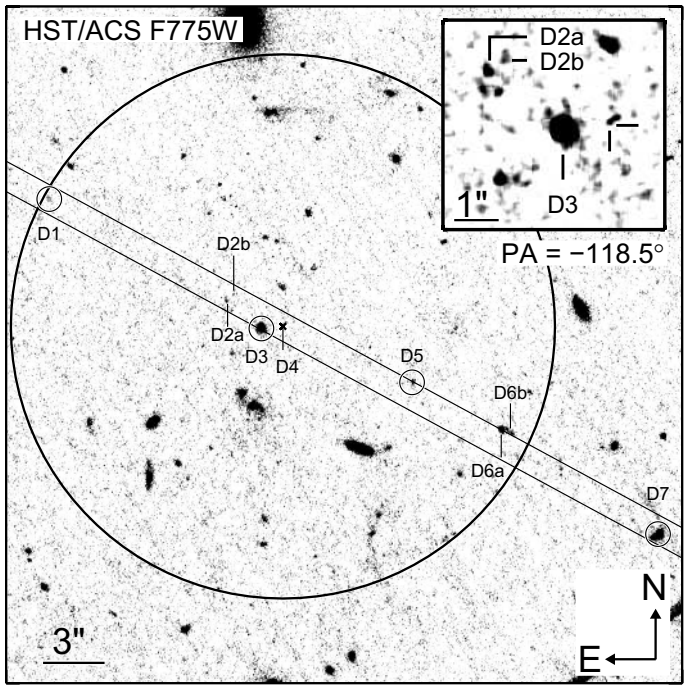

Fig. 6. Similar to Fig. 1, but for GRB 070721B ($z = 3.6298$). Object D4 is the host galaxy. Object D3 is the galaxy counterpart to the intervening DLA ($z = 3.094$) towards GRB 070721B. The impact parameter of the DLA galaxy is 1″ (7.9 kpc). The line of sight of object D7 also traverses a DLA at $z = 3.085$. The distance between objects D3 and D7 is 21.″6, corresponding to a projected distance of 167.4 kpc at $z = 3.09$. The inset is a 5″ zoom-in on the position of D3. The afterglow position is marked by the cross-hair.

4. Discussion

4.1. Detected galaxy counterparts

4.1.1. DLA galaxy towards GRB 070721B

In Sect. 3.4 we showed that the galaxy counterpart of the intervening DLA (object D3, $z_{\rm D3} = 3.096 \pm 0.003$) has an impact parameter of 7.9 kpc and an extinction-corrected R-band magnitude of 24.41 ± 0.02 mag (Fig. 6, Table 4). The co-ordinates are RA(J2000) $= 02^{\rm h}12^{\rm m}33\overset{\rm s}{.}018$ and Dec(J2000) $= -02^{\circ}11'40.''99$ with an uncertainty of 0.″4 in each coordinate. We denote the object as DLA J0212-0211 in the following. Up to now, only one other sub-DLA/DLA galaxy was identified beyond $z > 3$. Djorgovski et al. (1996) found the galaxy counterpart ($R = 24.8 \pm 0.2$ mag) to the $z = 3.15$ sub-DLA ($\log N$(H I) $= 20.0$; Lu et al. 1993) towards QSO B2233+131. Compared to typical $z \simeq 3$ galaxies, both objects are comparable to the brightness of an L_* galaxy ($R_* = 24.48 \pm 0.15$ mag; Steidel et al. 1999).

At low-z ($z < 1$), the overwhelming majority (75%) of sub-DLA/DLA galaxies summarised in Péroux et al. (2011) are fainter than the two $z > 3$ sub-DLA/DLA galaxies. The mean luminosity of that sample is 0.66 L_* and the median is 0.32 L_*. The sample is not tightly distributed around the mean and the brightest galaxy in that ensemble reaches 2.8 L_*. A proper comparison with high-z ($z > 2$) DLA galaxies is not possible. To date, the luminosity of only four out of ten sub-DLA/DLA galaxies is known. The reason for this is that most of them were detected by their Lyα emission and have small impact parameters so that they are outshone by the glare of the quasar. This hampers the determination of their luminosity. Chen et al. (2009) concluded that the DLA galaxy in the field of GRB 070721B is the most

[8] There are some uncertainties in the Lyα profile fits for D3, D4 and D7. Because of the resolution and the quality of the spectra, the damped wings are barely visible (see Fig. 5). We cannot rule out the possibility that a blend of narrow Lyα lines mimics the strong absorption feature. It is not very likely, because it would require that D3 and D7 have a comparable density of H I clumps at almost identical redshifts. Strictly speaking, the stated column densities are only upper limits. The fit does not rule out an extremely large Doppler parameter ($b \gg 100$ km s^{-1}), implying a reduction of the H I content by a factor of 100. This remark has in particular to be kept in mind for the strong Lyα absorption feature of the intervening absorber towards D7.

[9] We obtain the following 3σ upper limits from the VLT/FORS1 spectrum, assuming an aperture of 1665 km s^{-1} (twice the FWHM of a Gaussian with a Doppler parameter of $b = 500$ km s^{-1}): $EW_{\rm rest}$ (Si II λ1260) < 3.6 Å, $EW_{\rm rest}$ (O I λ1302) < 2.8 Å, $EW_{\rm rest}$ (C II λ1334) < 2.8 Å, $EW_{\rm rest}$ (Si IV λ1339) < 2.7 Å, $EW_{\rm rest}$ (C IV λ1548) < 2.7 Å, $EW_{\rm rest}$ (Fe II λ1608) < 3.0 Å, and $EW_{\rm rest}$ (Al II λ1670) < 3.3 Å. These limits are on average less stringent than the measurements of the detected metal lines in the DLA galaxy D3 (see Table 6).

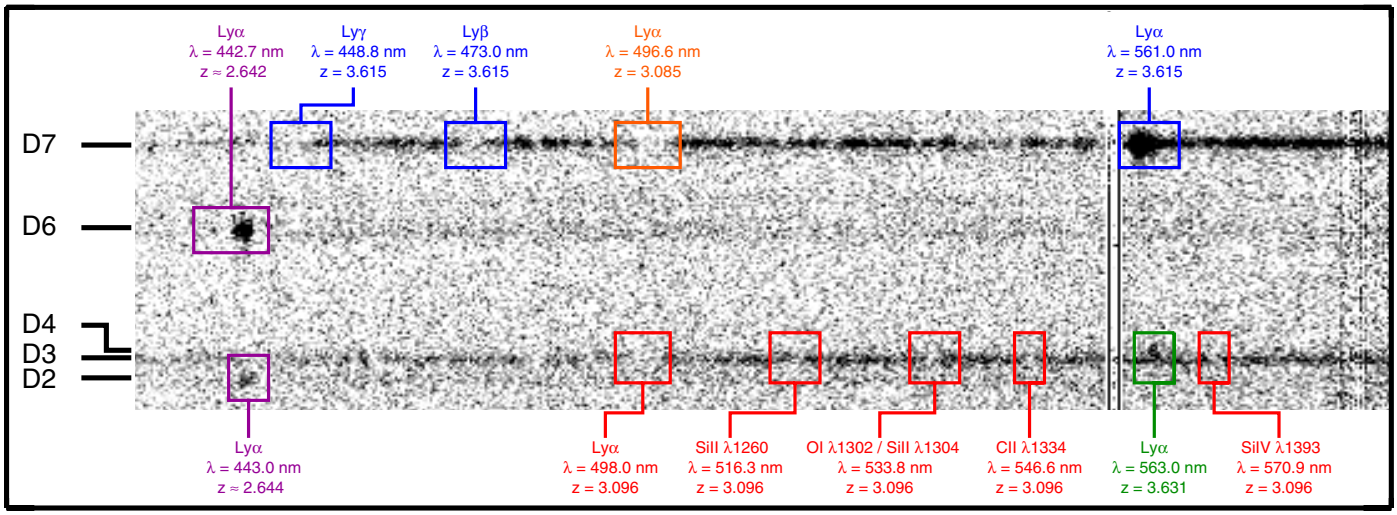

Fig. 7. VLT/FORS1 2D spectrum obtained after the optical afterglow of GRB 070721B faded. The photometric counterparts of the different traces are labelled according to Fig. 6 and Table 4. The host (D4) is only visible via its Lyα emission. The afterglow spectrum of GRB 070721B would be located at the position of D4. Prominent absorption and emission lines of the galaxies and intervening absorption-line systems are highlighted and colour-coded. The intervening DLA present in the afterglow spectrum is the very bright galaxy D3. The spectrum of the Lyα emitter D7 displays an intervening DLA as well.

luminous DLA galaxy at $z > 2$. The morphology of the galaxy is undisturbed, based on the shape in the HST image, inset in Fig. 6. We measure an ellipticity of 0.15 and a half-light radius of 1.2 kpc, obtained with `SExtractor`. The non-detection of a galaxy interaction or merger is not surprising. Overzier et al. (2010) argued that a detection is hampered at $z \sim 3$ because of the reduced physical resolution and sensitivity in addition to the general difficulties of observing interacting galaxies.

The Lyα absorption line shows an excess of flux in the red part of the absorption profile (Fig. 5; Sect. 3.4). The extracted emission line profile, shown in Fig. 8, is slightly asymmetric and peaks at $\sim$1000 km s^{-1} with respect to the systemic redshift. We measure a line flux density of $(2.34 \pm 0.25) \times 10^{-17}$ erg cm^{-2} s^{-1} Å^{-1}, i.e. a line significance of 9.2σ. Pettini et al. (1998a,b, 2000) reported the detection of the same feature with peak recessional velocities between +400 and 1100 km s^{-1} in several $z \approx 3$ galaxies (see also Adelberger et al. 2003). They argued that this feature is similar to a P-Cygni profile, indicating the presence of a galactic outflow (also found in starburst galaxies; e.g. Kunth et al. 1998; Gonzalez Delgado et al. 1998; but see also Verhamme et al. 2006; Laursen et al. 2009).

To explore the properties of the galaxy counterpart in more detail, we fitted the SED with `Le PHARE` (Sect. 2.3), as displayed in Fig. 8. Leaving all model parameters free except for the redshift, which was fixed to $z = 3.096$, the SED is best described by a young (0.4 Gyr) and close-to-dust-free galaxy ($A_V = 0.3$ mag, Calzetti reddening; see Table 5 for all best-fit values). The SFR of 37 $M_\odot$ yr^{-1} is similar to the that of the $z = 3.15$ DLA galaxy (Djorgovski et al. 1996; Christensen et al. 2004b; Péroux et al. 2011) and similar to the SFR of typical U-band drop-out LBGs (Giavalisco 2002).

Because of the small impact parameter of the DLA counterpart (1″), the GRB line-of-sight can be extinguished by the dust in the DLA galaxy if it contains dust (see Fynbo et al. 2011, for an example). Fynbo et al. (2009) derived the spectral slope between the optical and X-ray bands, β_{ox}, to be 0.72. According to Jakobsson et al. (2004), a dust-extinguished optical afterglow would result in $\beta_{ox} < 0.5$, which is not the case for GRB 070721B. Zafar et al. (2011) obtained a visual extinction of

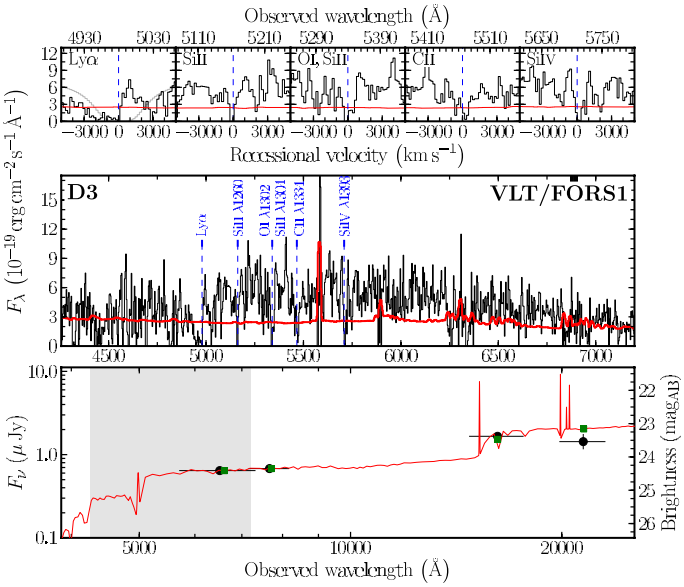

Fig. 8. Spectrum (*middle*) and the SED (*bottom*) of the DLA galaxy D3 in the field of GRB 070721B. In the *middle panel*, the error spectrum is overplotted and several absorption lines are marked. Regions of strong telluric features (atmosphere transparency <20%) were not used in the spectral analysis and are marked by a small box at the top. The *top panel* shows zoom-ins on the individual absorption lines. In the *bottom panel*, the observed extinction-corrected data points are shown as circles with error bars. The curve represents the best fit to the observed SED. The model-predicted magnitudes (squares) are superposed. The grey area highlights the interval that is covered by the spectrum above.

$A_V = 0.20 \pm 0.02$ mag, assuming that all extinction is attributed to an absorber in the host galaxy of GRB 070721B. This value is typical for GRB host galaxies (Kann et al. 2010; Schady et al. 2010; Zafar et al. 2011). Motivated by the fact that some GRBs show negligible host reddening, the presence of a foreground absorber cannot be excluded. Assuming the DLA to be responsible for the observed reddening, we expect that A_V increases only slightly (Greiner et al. 2011, their Fig. 3). Hence, we can in

Table 5. Properties of the galaxy counterpart candidates of the strong Mg II absorber towards GRB 050820A ($z_{\rm Mg\,II}$ = 0.692 and 1.430) and the DLA galaxy towards GRB 070721B ($z_{\rm DLA}$ = 3.094).

	GRB 050820A				GRB 070721B
	B2	B3	B5	B6	D3
z	0.693	$0.67^{+0.05}_{-0.06}$	$0.9^{+0.1}_{-0.2}$	$1.46^{+0.07}_{-0.41}$	3.096
θ (kpc)	87.5	36.8	26.4	42.0	7.9
M_B (mag)	−20.2	−19.4	−17.7	−21.4	−22.3
L/L_*	0.3	0.2	0.03	0.9	∼1
Dust model			Calzetti		
A_V (mag)	0.3	1.6	0.3	0.3	0.3
Age (Gyr)	2.0 ± 0.2	$1.3^{+2.3}_{-0.7}$	$0.6^{+1.3}_{-0.4}$	$0.5^{+0.5}_{-0.1}$	$0.4^{+0.5}_{-0.2}$
log $M/M_\odot$	10.3 ± 0.1	$9.9^{+0.2}_{-0.1}$	8.4 ± 0.2	10.1 ± 0.1	$10.1^{+0.3}_{-0.2}$
SFR $\left(M_\odot\,{\rm yr}^{-1}\right)$	$0.15^{+0.03}_{-0.02}$	7.5 ± 2.7	$0.5^{+1.2}_{-0.3}$	$1.5^{+1.5}_{-0.6}$	37^{+117}_{-23}
χ^2/n.o.f.[a]	16.3/9	7.3/9	1.5/5	1.6/9	5.0/4

Notes. Summary of the most important properties of the SED fits of the most likely candidates. The redshifts of B2 and D3 were fixed to the spectroscopically measured redshift in the SED fit. The impact parameters, θ, were calculated from Table 4, assuming either z = 0.6915, 1.430, or 3.096. The luminosities were computed using the results by Dahlen et al. (2005) and Steidel et al. (1999) on LFs; the knee of the luminosity functions L_* is at $M_{B,*}$ = −21.43 M_B = −21.60 and m_R = 24.48 mag at z = 0.692, 1.4288 and 3.096, respectively. We note that the stellar mass and its uncertainty were derived assuming a Chabrier IMF (Chabrier et al. 2000, see also Sect. 2.3 for more details on the SED fit). [(a)] "n.o.f." stands for number of filters.

this case exclude the presence of significant amounts of dust, i.e. $A_V < 0.20$, in the outskirts of the DLA galaxy.

In addition, we measured the *EW*s of absorption lines in the DLA galaxy spectrum D3 and of absorption lines imprinted by the DLA galaxy on the GRB afterglow spectrum. The EWs and column density estimates are listed in Table 6. By comparing the two sets of data it is evident that the DLA galaxy shows a higher N (H I) than in the afterglow spectrum (see Fig. 5). This trend is also confirmed by all metal EWs, which are higher for the DLA galaxy, despite the individual large errors. These results are easily explained if most of the DLA galaxy light arises from the central, i.e. denser, region of the galaxy, while the GRB afterglow radiation shone through a more peripheral region of the host.

Finally, the most constraining metallicity estimate for the D3 galaxy is [Fe/H] > −0.21 (measured from the GRB afterglow spectrum). Because iron is a very refractory element, a significant amount of Fe could be depleted onto dust grains and not observed in the gas-phase. If this is the case, the intrinsic metallicity would increase to solar or super-solar values, while GRB DLAs typically show solar or sub-solar metallicities (see Fynbo et al. 2009, and references therein). A more likely scenario is a limited amount of dust in the DLA galaxy, which is supported by the low reddening along the line-of-sight ($A_V < 0.20$) estimated from the SED. Thus, the metallicity along the GRB line-of-sight, i.e. 7.9 kpc away from the galaxy centre, is close to $\approx 0.6\,Z_\odot$. A higher metallicity could possibly be found in the central regions of the DLA galaxy, given the likely metallicity gradient, but cannot be constrained from our dataset due to absorption-line saturation.

In conclusion, the properties of the DLA galaxy D3 are very typical for LBGs, except that the halo of the galaxy harbours large amounts of neutral hydrogen. This is consistent with the model that DLAs are gaseous halos of faint high-z LBGs (Fynbo et al. 1999; Møller et al. 2002; Fynbo et al. 2008; Rafelski et al. 2011).

4.1.2. Mg II absorbers towards GRB 050820A

In addition to the intervening sub-DLA towards GRB 050820A, the afterglow traverses two strong Mg II absorbers at z = 0.6915 and 1.4288 (see Table 3). We find four galaxies within 100 kpc that are consistent with either z = 0.6915, namely B2, B3 and B5 (Figs. A.2–A.4, Table 4), or z = 1.4288, namely B6 (Fig. A.5, Table 4)[10]. The properties of the best-fit galaxy templates are summarised in Table 5[11].

The impact parameters vary between 26 and 88 kpc for the candidates of the Mg II absorber at z = 0.6915. Galaxy counterparts with an absorption cross-section of more than 88 kpc are rare; for instance Chen et al. (2010) used a set of 94 galaxies ($\langle z\rangle$ = 0.24) that are located up to 120 kpc around 70 background quasars ($z_{\rm QSO} > 0.6$) to study which kind of Mg II absorber could be found in the quasar spectrum arising from these galaxies. They did not find any strong Mg II absorber in a quasar spectrum that is related to a galaxy at a distance of more than ∼40 kpc from the line of sight of the quasar. Hence, the early-type galaxy B2 is probably not the galaxy counterpart of the absorption-line system. The impact parameters of B3 and B5 are typical for strong Mg II absorbers (Chen et al. 2010), though at the upper end of the impact parameter distribution. The properties of B3 and B5 are very different from each other (Table 5), B3 is a massive galaxy with a high SFR, while B5 is a young low-mass galaxy with low SFR. These differences are also reflected in their luminosities; adopting the Dahlen et al. (2005) LF, B3 is 0.2 L_*, and B5 is 6 times fainter (0.03 L_*). Both values are in the range of the observed luminosities of the Chen et al. (2010) sample, but in their fainter half.

Galaxy B6 is the most likely galaxy counterpart of the strong Mg II absorber at z = 1.4288. The impact parameter of 42 kpc (4.″9; Table 5) is similar to the impact parameter of the galaxy counterpart candidates of the Mg II absorber at z = 0.6915. The properties of the best-fit galaxy template, displayed in Table 5, show that it is a fairly bright (0.9 L_*) galaxy with SFR = 1.5 $M_\odot\,{\rm yr}^{-1}$ (Fig. A.5).

Without additional spectroscopic data it is not possible to decide which of two candidates is the galaxy counterpart of the strong Mg II absorber z = 0.6915 and if B6 is the galaxy counterpart to the Mg II absorber at z = 1.4288. Chen (2012) placed an upper limit on the brightness of the galaxy counterpart of $F775W$ = 27.5 mag, i.e. fainter than a 0.03 L_* galaxy, if the impact parameter is less than 3.″5.

4.2. Limits on galaxy counterparts

In the previous sections we discussed the properties of the detected DLA galaxy towards GRB 070721B and of the galaxy counterpart candidates of the two strong Mg II absorbers towards GRB 050820A. In this section we present the limits, such as luminosity and SFR, on the non-detected galaxy counterparts. The limits on the luminosities shown in Table 7 are related to the knee of the Dahlen et al. (2005) and the Reddy et al. (2008) LFs. The galaxy counterparts are fainter than a 0.5 L_* and 1.5 L_* galaxy in all fields, if the impact parameter is 50 and 100 kpc, respectively. The most stringent upper limit of 0.1 L_* can be placed on the galaxy counterparts of the intervening sub-DLA towards

[10] The photometric redshift of B6 also matches that of a weak Mg II absorber at z = 1.6204 towards GRB 050820A. It is unlikely that the galaxy is the counterpart of the weak Mg II absorber, because the correlation length of weak Mg II absorbers is ∼2 kpc (Ellison et al. 2004).

[11] We recall that the solution of B5 is not unique, because it is only detected in five filters.

Table 6. DLA J0212-0211 absorption lines in the DLA galaxy and the GRB 070721B afterglow spectrum.

Ion	Transition (Å)	$EW_{\rm rest}$ [a] (Å)	log N	[X/H]	$EW_{\rm rest}$ [a] (Å)	log N	[X/H]
		Spectrum of the DLA galaxy D3			**D3 in the afterglow spectrum**		
H I	1215		21.3 ± 0.2[b]			20.1 ± 0.3[b]	
Si II	1260	3.00 ± 0.98	>14.32[c]	>−2.49	<2.44	...	...
O I/Si II	1302/1304	3.94 ± 1.15	...	...	3.06 ± 0.83	...	...
C II	1334	3.97 ± 1.11	>15.29	>−2.44	<3.57	...	...
Si IV	1393	3.41 ± 1.01	>14.57	...	<2.59	...	...
Si II	1526	<5.05	...	...	2.35 ± 0.69	>1495[c]	>−0.66
C IV	1548/1549	<6.13	...	...	4.34 ± 0.73	>1503	...
Fe II	1608	<4.98	...	...	3.02 ± 0.62	>1539	>−0.21
Al II	1670	<7.33	...	...	2.33 ± 0.74	>1370	>−0.85

Notes. The last column denotes the metal abundance with respect to solar. [(a)] The restframe EW (1σ errors) and the 3σ detection limits are measured assuming an aperture of 1665 km s^{-1}, i.e. twice the full width at half maximum of a Gaussian with Doppler parameter b = 500 km s^{-1}. [(b)] Derived from the Voigt profile fit of the Lyα absorption, see Fig. 5. [(c)] The column densities, derived from the EW in the optically thin limit, are considered as lower limits because the lines are saturated.

Table 7. Limiting magnitudes of the galaxy counterparts of the intervening absorption line systems.

Absorber	$z_{\rm abs}$	$F775W_{\rm UL}$ (mag) for θ < 50 (100) kpc	L/L_*	Fynbo model
GRB 050730 ($z_{\rm GRB}$ = 3.969)				
DLA	3.56439	>25.7/>24.6	<0.5/<1.5	<0.04
sub-DLA	3.02209	>25.7/>24.6	<0.4/<1.1	<0.04
Mg II	2.25313	>26.5/>25.1	<0.2/<0.5	
Mg II	1.7743	>26.5/>25.1	<0.1/<0.5	
GRB 050820A ($z_{\rm GRB}$ = 2.615)				
sub-DLA	2.3598	>26.7/>26.7[a]	<0.1/<0.1	<0.1
GRB 050908 ($z_{\rm GRB}$ = 3.3467)				
sub-DLA	2.6208	>25.0/>24.7[b]	<0.4/<0.6	≳ 0.5
Mg II	1.5481		<0.3/<0.4	

Notes. Limiting magnitudes corrected for Galactic extinction. We adopted the Dahlen et al. (2005) and Reddy et al. (2008) LFs to relate an absolute magnitude with the knee of a corresponding LF, L_*: 1.59 < z < 1.9: M_* = −20.69 ± 0.26 mag (U-band), 1.9 ≤ z < 2.7: M_* = −21.01 ± 0.38 mag (1700 Å), 2.7 ≤ z < 3.4: M_* = −20.84 ± 0.12 mag (1700 Å). We extended the range of the LFs from z = 1.59 to 1.50 and from z = 3.4 to 3.56, because the change in the M_* is smaller than its uncertainty. To compute the absolute magnitude we used $M = m - DM(z) + 2.5\log(1+z)$, where $DM(z)$ is the distance modulus. Different filters than $F775W$ were used if a filter was closer to the central wavelength of the LF than the $F775W$ band. In the column "Fynbo model" we display the limits on the luminosity of DLA galaxies based on the model by Fynbo et al. (2008). [(a)] The $F625W$ magnitude was used. [(b)] The R-band magnitude was used.

GRB 050820A. For this field, Chen (2012) reported that the galaxy counterpart is fainter than $F775W$ = 27.5 mag, corresponding to 0.06 L_*, if the impact parameter is smaller than 3.″5.

Fynbo et al. (1999) suggested that DLAs are the gaseous halos of LBG (see also Møller et al. 2002; Fynbo et al. 2008; Rafelski et al. 2011). To compare our measurements with this model, we use the predictions on the brightness of galaxy counterparts by Fynbo et al. (2008). In their model, simple and constrained scaling relations of galaxies in the local Universe are used to predict the luminosity of intervening DLAs based on their metallicity and their impact parameter. These relations are strictly speaking only valid for $z \sim 3$ DLAs. We also adopted this model for DLAs at lower redshift and for sub-DLAs. The main difference between a sub-DLA and a DLA is a larger covering fraction, i.e. impact parameter, if DLAs and sub-DLA are drawn from the same population of galaxies. Based on the measured metallicities, we estimated the brightness and the impact parameter of the unidentified DLA galaxies towards GRBs 050730 and 050820A. For GRB 050908, we used $EW_{\rm rest}$ (Si II λ1526) as a metallicity proxy (Prochaska et al. 2008).

The estimated brightnesses, shown in Table 7, indicate that most galaxy counterparts evaded detection because of their intrinsic faintness. This result is not surprising. The majority of all $z \sim 3$ DLA galaxies are expected to be fainter than ∼29.5 mag in the R-band, i.e. $L \lesssim 0.012\,L_*$, in the Fynbo et al. (2008) model. The model clearly rules out large impact parameters. Even the larger covering fraction of sub-DLAs does not imply impact parameters of more than 2–3″ (15.7–23.5 kpc at $z \sim 3$). The intervening DLA towards GRB 050908 possibly has a ∼0.5 L_* galaxy counterpart.

We find several objects in the field of GRBs 050730 and 050908 that fulfil both criteria, being very faint and having a very small impact parameter (Table 4). There are several objects with a brightness of $F775W \sim 28.4$ mag within 2.″5 of the afterglow position of GRB 050730. If one of these objects is the galaxy counterpart to the sub-DLA, it is a 0.03 L_* galaxy. In the field of GRB 050908 we find four objects ranging in brightness from R = 25.3 to 27 mag within 4″ of the afterglow position, corresponding to $L \lesssim 0.4\,L_*$. To elucidate the nature of these objects, more data are required.

4.3. Quasar radiation field

In Sect. 3.1, we alluded to the serendipitous coincidence of the sub-DLA (z = 3.02) towards GRB 050730 and the QSO that is 17.″5 south of the GRB position. Before we discuss their connection, we present general properties of the quasar.

After subtracting the bright R = 18.2 mag foreground star (Sect. 2.2; Table 4), we measure an R-band magnitude of 20.78 ± 0.05 mag (corrected for Galactic extinction, Table 4). The coordinates of the quasar are RA(J2000) = $14^{\rm h}08^{\rm m}17.^{\rm s}135$ and Dec(J2000) = −03°46′35.″35, with an uncertainty of 0.″4. Hereafter the QSO is denoted as QSO J1408-0346. Figure 9 shows the quasar spectrum secured with X-shooter on

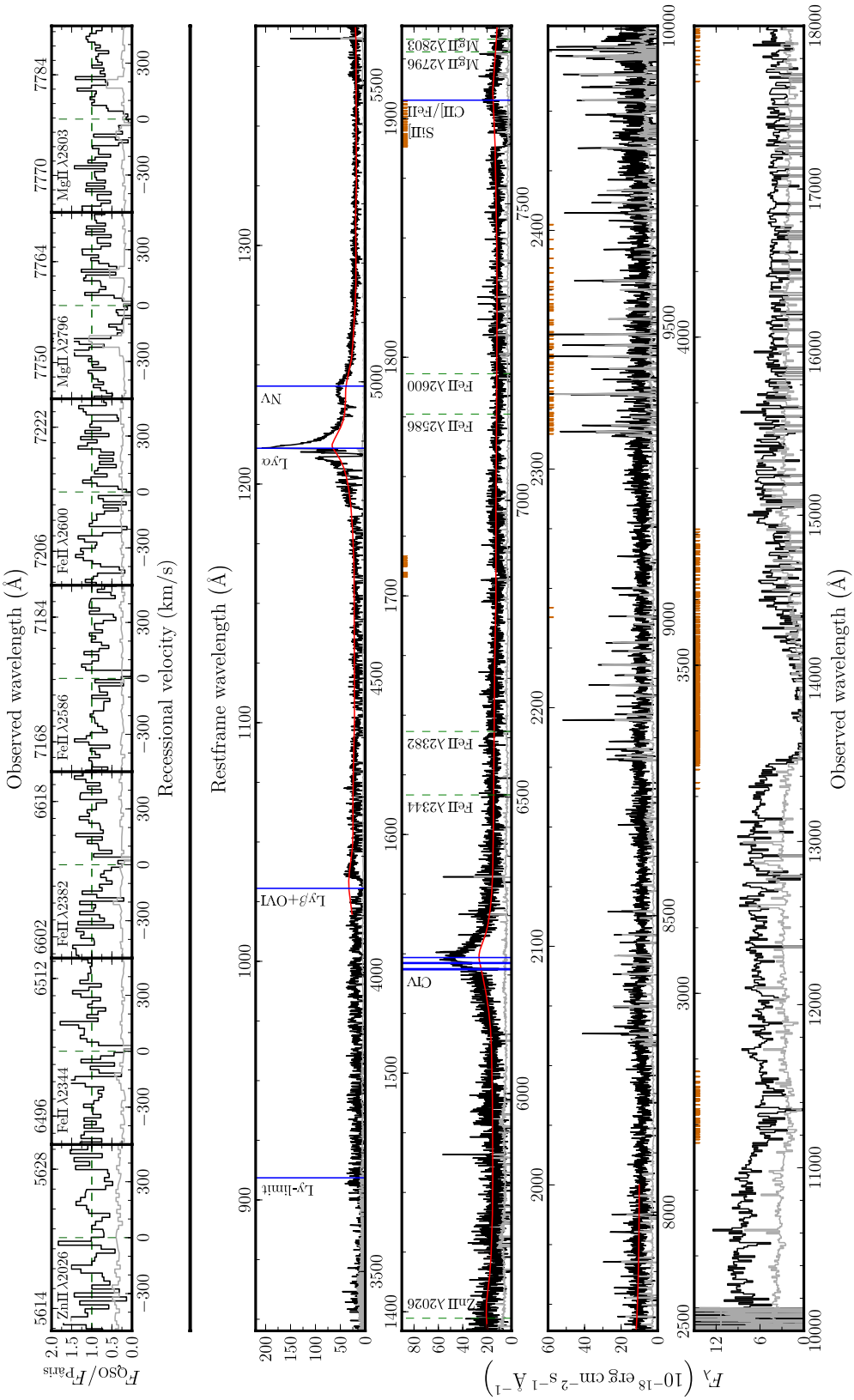

Fig. 9. X-shooter spectrum of QSO J1408-0346 (*bottom*). The spectrum beyond 1.8 μm is not shown due to uncertainty in the flux calibration. The observed and rest-frame wavelengths are shown below and above each panel, respectively. The error spectrum is shown in grey. Regions of strong telluric features (atmosphere transparency <20%) were not used in the spectral analysis and are marked by small boxes at the top of each panel (NIR: Gemini observatory). The red line is the average $z = 3$ QSOs spectrum taken from Pâris et al. (2011). Prominent absorption and emission lines from the quasar are indicated by vertical solid lines, and the absorption lines from the strong Mg II absorber at $z = 1.77425$ by vertical dashed lines (see Table 8). Zoom-ins on the absorption lines of the Mg II absorber are shown in the top panel. They were normalised with the QSO composite spectrum.

Table 8. Absorption and emission lines of QSO J1408-0346 and the strong Mg II absorber at $z = 1.77425$ towards it.

λ_{obs} (Å)	λ_{rest} (Å)	Species	Redshift	$EW_{rest}{}^a$ (Å)
3658	911.20	Ly-limit	3.01	
≈4168.8	**≈1033**	**Lyβ + O VI**	**≈3.04**	
4888	**1215.80**	**Lyα**	**3.02**	
4992.72	**1239.42**	**N V**	**3.028**	
5621.30	2026.14	Zn II	1.77425	<0.73
6208.75	1548.20	C IV	3.010	
6210.62	1548.20	C IV	3.011	
6219.37	1550.77	C IV	3.010	
6220.87	1550.77	C IV	3.011	
6229.35	**1545.86**	**C IV**	**3.030**	
6503.52	2344.21	Fe II	1.77425	<0.49
6610.51	2382.77	Fe II	1.77425	0.84 ± 0.15
7145.59	2586.65	Fe II	1.77425	<0.54
7213.61	2600.17	Fe II	1.77425	0.62 ± 0.19
≈7674.8	**≈1910**	**Si II, C III/Fe II**	**3.018**	
7756.18	2796.35	Mg II	1.77425	1.24 ± 0.34[b]
7777.52	2803.53	Mg II	1.77425	1.25 ± 0.19

Notes. Summary of the most important absorption and emission lines of the quasar and the strong Mg II absorber at $z = 1.77425$. We show only those absorption lines that are redward of the quasar Lyα emission line. Emission lines are displayed in bold. [(a)] The restframe EWs (1σ errors) and the 3σ detection limits are measured assuming an aperture of 333 km s^{-1}, i.e. $2 \times FWHM$ a Gaussian with Doppler parameter b = 100 km s^{-1}. [(b)] The EW of the lines of the Mg II doublet are similar, indicating that the lines are saturated.

18 April, 2010. Table 8 summarises the detected quasar emission and absorption lines; the mean emission line redshift is $z_{em} = 3.023 \pm 0.007$. The emission lines are substantially narrower in comparison to the quasar composite spectrum by Pâris et al. (2011), which is overplotted in red. In addition to the emission lines, we detect C IV and Lyα in absorption at z_{qso} (Table 8). The narrow C IV absorption lines consist of two blueshifted velocity components at 1420 and 1497 km s^{-1} with respect to the maximum of the C IV emission line.

The proximity of the GRB line-of-sight can constrain the quasar radiation field. Fox et al. (2007) reported that DLAs and sub-DLAs bearing N V are extremely rare, and that several of these have a nearby QSO coincident (>33%) at the (sub)-DLA redshift (see also Fox et al. 2007; Ellison et al. 2010). We did not find evidence for N V in absorption in the GRB afterglow spectrum. Addditionally, the ionising UV radiation field of a bright quasar can also lead to visible underdensity in the Lyα forest as the redshift approaches the quasar emission redshift. This is referred to as the proximity effect (Carswell et al. 1982; Tytler 1987; Bajtlik et al. 1988). In addition, if the quasar radiates isotropically, the line of sight of GRB 050730 might show an underdensity in the Lyα forest around the redshift of the foreground quasar (i.e. the transverse proximity effect; Bajtlik et al. 1988). At the projected distance of 137 kpc, the QSO with an inferred Lyman-limit flux density of 9 μJy exceeds the H I UV background at $z \sim 3$ by a factor of ∼170 (Guimarães et al. 2007; Dall'Aglio et al. 2009). In this case, the Lyα forest at the redshift of the QSO is dominated by the sub-DLA so it impossible to infer if there is an effect of the QSO on the IGM along the GRB afterglow line-of-sight.

4.4. Correlated structures

The spectra of GRB 050730 and the QSO 17.″5 south of it (Fig. 1) share a common wavelength interval, as do GRB 070721B and the bright galaxy D7 20.″7 SW of it (Fig. 6). These allow us to identify correlated structures in both fields. We are particularly interested in absorbers with metal lines, because they are related to galaxies. Their detections provide information on galaxy impact parameters and their clustering.

Correlated structures have been found in several quasar pairs on a length scale of a few kpc up to ∼100 kpc (e.g. Smette et al. 1995; Petry et al. 1998; Ellison et al. 2004, 2007), and on a length scale of several hundreds of kpc up to a few Mpc (Francis & Hewett 1993; Francis et al. 1996; Fynbo et al. 2003; D'Odorico et al. 2002; Coppolani et al. 2006). In the literature, two different scenarios are discussed to explain correlated structures on these different length scales: a) the lines of sight probe the halo of one galaxy, or of a galaxy and a satellite galaxy; and b) the different lines of sight probe different galaxies that belong to a group of galaxy and are part of a large-scale structure. Here we argue that the latter interpretation of correlations being due to large scale structure better explains our observations of the absorbers in both GRB fields.

4.4.1. The field of GRB 050730

The lines of sight of GRB 050730 and QSO J1408-0346 are separated by 17.″5. We identify a Mg II at $z \approx 1.774$ in both of them, as well as the sub-DLA towards the GRB and QSO J1408-0346 that are at almost identical redshifts ($z_{sub-DLA} = 3.02209$, $z_{QSO,em} = 3.023$).

The coincidence of the sub-DLA and the QSO is in line with evidence for anisotropic emission of QSOs, which seem to have cleared their surroundings preferentially towards us rather than perpendicular to the line-of-sight (Hennawi & Prochaska 2007). At least it suggests that QSOs reside in overdense regions (Rollinde et al. 2005; Faucher-Giguère et al. 2008). The angular distance of 17.″5 between the sub-DLA and the QSO translates into a transverse distance of 137 kpc at $z \simeq 3.022$, which is several times larger than the typical sub-DLA impact parameter of ∼39 kpc in Péroux et al. (2011) and Krogager et al. (2012). Ellison et al. (2010) argued that proximate DLAs, i.e. DLAs within a comoving distance of 42 Mpc ($\Delta v = 3000$ km s^{-1}) around QSOs, are not associated with the QSO host, but rather sample overdensities around it (see also Russell et al. 2006). Therefore, the intervening sub-DLA towards GRB 050730 could be an overdensity in the vicinity of the QSO rather than a part of the massive halo of the quasar host galaxy.

The common Mg II absorbers towards GRB 050730 and the QSO are at $z_{GRB,Mg II} = 1.7731$ and $z_{QSO,Mg II} = 1.77425$. Vergani et al. (2009) reported a restframe Mg II equivalent width of 0.93 ± 0.03 Å and Prochaska et al. (2007a) reported that the doublet is saturated so that the absorber can be placed in the strong Mg II absorber category. For the intervening Mg II absorber towards the QSO, we measure $EW_{rest}(2796\,Å) = 1.24 \pm 0.34$ (saturated; Table 8). In addition, we detect Zn II λ 2026 and several Fe II absorption lines of that absorber at the same redshift, summarised in Table 8. At the redshift of 1.774, the angular distance of 17.″5 translates into a projected distance of 150 kpc, while their redshift implies a velocity distance of 124 km s^{-1}. Chen et al. (2010) reported a typical impact parameter of around ∼30 kpc for Mg II absorbers (see also Smette et al. 1995), arguing against the hypothesis that both strong Mg II absorbers are

associated with the same galaxy[12]. Finally, we note that there is a high-column density absorber at $z \approx 2.98$ in the afterglow spectrum, which has no counterpart in the spectrum of the quasar.

4.4.2. The field of GRB 070721B

In Sect. 3.4 we identified object D3 as the galaxy counterpart of the intervening DLA in the afterglow spectrum of GRB 070721B. In addition, we identified another intervening DLA towards the Lyα emitter D7 that is at a similar redshift and has a similar H I column density to the DLA galaxy, but is 160.7 kpc from the location of D3 (Figs. 5, 6). It is unlikely that the intervening DLA towards D7 is gravitationally bound to the DLA galaxy D3 because of this large impact parameter. The average impact parameter of DLAs is 13 kpc, although Francis et al. (1996) also reported a candidate counterpart with impact parameter of 182 kpc.

D3 and the intervening absorber towards D7 appear more similar to the pairs of intervening absorption-line systems discussed in Ellison et al. (2007)[13]. They found found a pair of sub-DLAs at $z = 2.94$ and a pair of DLAs at $z = 2.66$ towards a binary quasar, where the individual absorbers of each pair are separated by ∼100 kpc. Based on simulations, they showed that the presence of a large-scale structure is more likely than the different lines of sight probing the halo of two massive galaxies at $z = 2.66$ and 2.94, respectively. In this case, the probability increases from $p \lesssim 10^{-3}$ to 0.01. We find several correlated structures on a length scale of ∼160 kpc in the fields of GRBs 050730 and 070721B. These are most likely more examples for a group environment of intervening absorption-line systems.

5. Conclusions

The aim of our work was to detect galaxy counterparts of high-z intervening sub-DLAs and DLAs. In contrast to previous studies, we used GRBs to have a clear view on the region that is usually outshone by the glare of a quasar. Since the launch of the *Swift* satellite, seven intervening sub-DLAs and DLAs have been found towards six GRBs. Among them, four lines-of-sight have sufficient photometric and spectroscopic data to study very faint objects.

In our study we successfully detected the DLA galaxy that causes the intervening DLA absorption towards GRB 0707021B, 1″ from the afterglow position, as suggested by Chen et al. (2009) and Fynbo et al. (2009). However, these authors did not present any spectroscopic evidence for their inference. Indeed, the DLA galaxy would have been almost impossible to detect by direct imaging if the background source had been a 19-mag quasar. This underlines the argument of Jakobsson et al. (2004) that studies of the galaxy counterparts of intervening absorption line systems towards QSOs can be affected by misidentifications. Hence, proximity is not sufficient for an association. For instance in the case of GRB 050820A, the extensive photometric and spectroscopic campaigns allowed us to successfully rule out all objects brighter 26.2 mag in $F625W$-band within 3.″7, corresponding to $L \lesssim 0.1\,L_*$ at $z = 2.3598$. Assuming that sub-DLAs and DLAs are LBGs weighted by their H I cross-section, Fynbo et al. (2008) showed that the overwhelming majority of intervening DLA galaxies are expected to be fainter than this, naturally explaining the non-detections. Even with the largest telescopes, it is difficult to detect and elucidate the nature of these faint objects. On the other hand, there are cases where intervening absorption-line systems were successfully associated with galaxies at larger distances (e.g. Francis & Hewett 1993), however they are just a minority.

The disadvantage of our approach is the vast amount of observing time required. Deep multi-filter observations exist for several GRBs. However, similar extensive spectroscopic campaigns do not exist for other GRB fields. In those cases, one relies on SED fitting techniques. Rao et al. (2011) showed that this can indeed be successful, in particular for very faint objects where only emission-line spectroscopy is feasible. Recently, Péroux et al. (2011) performed a survey for galaxy counterparts of intervening DLAs using the integral field unit VLT/SINFONI (see also Christensen et al. 2004a; Bouché et al. 2012). This approach could be complementary to the classical strategy of performing very deep imaging campaigns and spectroscopic follow-ups on candidates, or the use of narrow band and broad band strategy to search for emission line objects (e.g. Vreeswijk et al. 2003).

The DLA galaxy ($z = 3.096 \pm 0.003$) in the field of GRB 070721B is the most luminous high-z DLA galaxy known (Chen et al. 2009), and is almost as distant as the highest-redshift DLA galaxy known so far at $z = 3.15$. The number of high-z sub-DLA and DLA galaxies increases thus from nine to ten. DLA J0212-0211 is very metal rich, [Fe/H] > -0.21. It does not differ from normal LBGs, with the exception of the large amount of H I in its halo. This supports a model in which DLAs can be gaseous halos of LBGs (Fynbo et al. 1999; Møller et al. 2002; Fynbo et al. 2008; Rafelski et al. 2011).

The extensive photometric and spectroscopic campaigns allowed us to identify galaxy counterpart candidates of two strong Mg II absorbers at $z = 0.6915$ and 1.4288 towards GRB 050820A. The most likely candidates have impact parameters between 36.8 and 42.0 kpc, which is in the expected range of Mg II absorbers (Chen et al. 2010). Their properties point to young star-forming galaxies, ranging in luminosity from $0.2\,L_*$ to $0.9\,L_*$.

Finally, we studied the presence of correlated structures as a particular class of intervening absorption-line systems, a phenomenon observed in the field of GRBs 050730 and 070721B. We found evidence for three correlated structures in the field of GRB 050730 and one in the field of GRB 070721B. These absorbers range in redshift from $z = 1.774$ to 3.096 and were probed over transverse distances between 137 and 161 kpc. All of them have associated metal absorption-lines. It is unlikely that the objects in these correlated structures are gravitationally bound to each other, based on simulations (e.g. Ellison et al. 2007). The detection is nevertheless intriguing. The average distance between quasar pairs is several times larger. Up to now, intervening absorption-line systems with coincidences in redshift have been found with separations of several hundreds of kpc up to a few Mpc (e.g. Francis & Hewett 1993; D'Odorico et al. 2002), but only few with a separation of ∼150 kpc (Ellison et al. 2007). These serendipitous discoveries are important for studying the absorption cross-section of intervening absorption-line systems, their correlation length, and their implications on galaxy groups in the early Universe.

[12] The galaxy counterpart of the Mg II absorber towards the QSO is fainter than 26.5 (25.1) mag in $F775W$ (corrected for Galactic extinction) for an impact parameter of 50 kpc (100 kpc), assuming that the galaxy counterpart is neither in the glare of the QSO, nor at the position of the foreground star. Adopting the Dahlen et al. (2005) LF, the limiting magnitudes correspond to $L < 0.13\,L_*$ and $L < 0.48\,L_*$.

[13] The galaxy counterpart of the intervening DLA towards D7 is fainter than 25.2 mag in $F775W$, assuming an impact parameter of 50 to 100 kpc, corresponding to $L < 0.7\,L_*$, using the LF in Reddy et al. (2008).

Acknowledgements. We thank the referee for a careful reading of the manuscript and for helpful comments that improved this paper. S.S., A.D.C. and P.J. acknowledge support by a Grant of Excellence from the Icelandic Research Fund. J.P.U.F. acknowledges support form the ERC-StG grant EGGS-278202. A.R. acknowledges support by the Thüringer Landessternwarte Tautenburg and by the Graduierten-Akademie Jena, Germany. S.S. thanks D. Malesani (Dark Cosmology Centre, Copenhagen) for many productive and valuable discussions and D. A. Kann (Thüringer Landessternwarte Tautenburg, Germany) for corrections and comments on the manuscript.

Appendix A: Additional figures

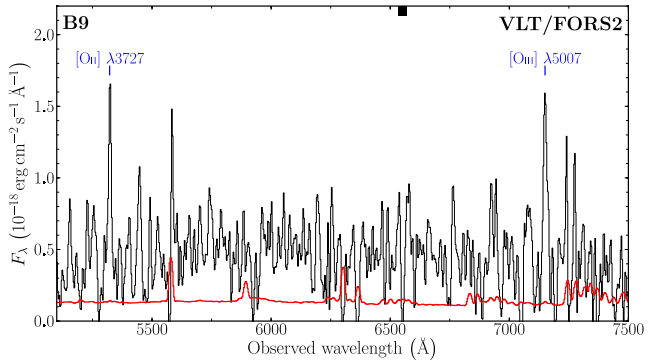

Fig. A.1. Smoothed spectrum of the galaxy B9 in the field of view of GRB 050820A. Based on the identification of [O II] λ3727 and [O III] λ5007 the redshift is $z = 0.428$. The galaxy is not related to any of the intervening absorbers seen in the afterglow spectrum. The error spectrum is overplotted. Regions of strong telluric features (atmosphere transparency <20%) were not used in the spectral analysis and are marked by small boxes at the top.

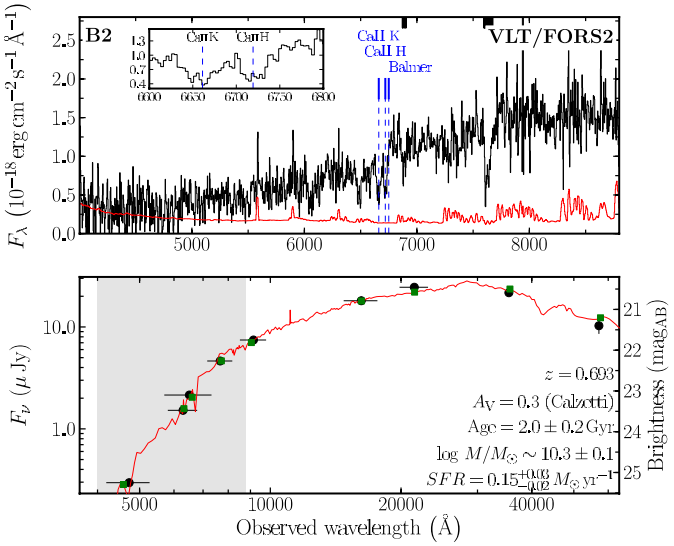

Fig. A.2. Galaxy B2 in the field of GRB 050820A. *Top*: spectrum acquired with VLT/FORS2. The identified Ca II H&K absorption lines and the Balmer break are marked. The inset zooms-in on the position of the both absorption lines. Based on the identification of the three absorption features the redshift of the galaxy is $z = 0.693$. The error spectrum is overplotted. Regions of strong telluric features (atmosphere transparency <20%) are not used in the spectral analysis and are marked by small boxes at the top. *Bottom*: SED from g'-band to 5.8 μm. The observed data points (corrected Galactic extinction) are shown as circles with error bars. The solid line displays the best-fit model of the SED ($\chi^2 = 16.3$; number of filters =9). The model-predicted magnitudes are superposed (squares). The grey area highlights the interval that is covered by the spectrum above.

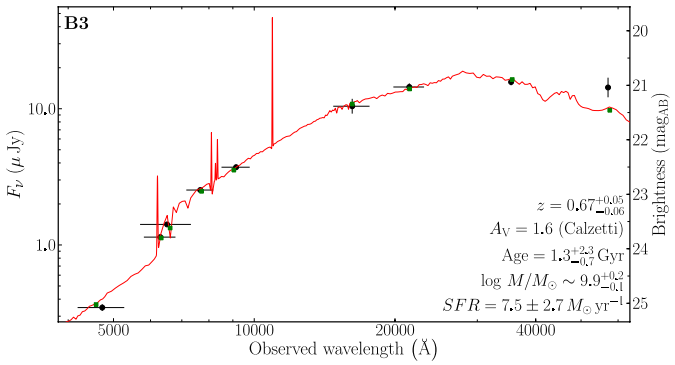

Fig. A.3. Similar to Fig. A.2, but for galaxy B3 from g'-band to 5.8 μm. The fit quality is $\chi^2 = 7.3$ for nine filters.

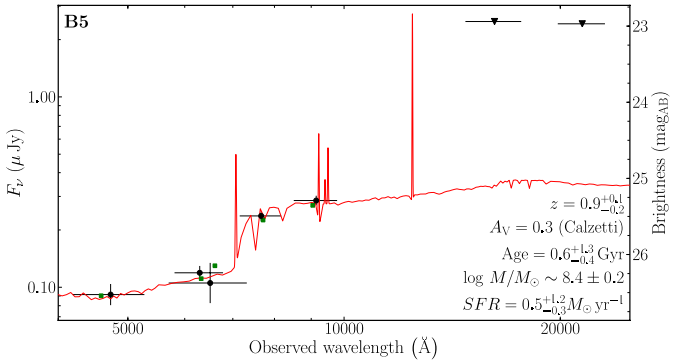

Fig. A.4. Similar to Fig. A.2, but for galaxy B5 from g'- to K_s-band. The fit quality is $\chi^2 = 1.5$ for five filters.

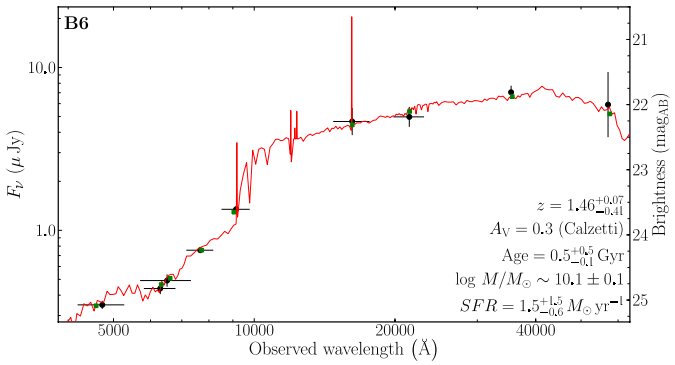

Fig. A.5. Similar to Fig. A.2, but for galaxy B6 from g'-band to 5.8 μm. The fit quality is $\chi^2 = 1.6$ for nine filters.

References

Adelberger, K. L., Steidel, C. C., Shapley, A. E., & Pettini, M. 2003, ApJ, 584, 45
Adelberger, K. L., Steidel, C. C., Kollmeier, J. A., & Reddy, N. A. 2006, ApJ, 637, 74
Arnouts, S., Cristiani, S., Moscardini, L., et al. 1999, MNRAS, 310, 540
Asplund, M., Grevesse, N., Sauval, A. J., & Scott, P. 2009, ARA&A, 47, 481
Bajtlik, S., Duncan, R. C., & Ostriker, J. P. 1988, ApJ, 327, 570
Bertin, E., & Arnouts, S. 1996, A&AS, 117, 393
Blanton, M. R., & Roweis, S. 2007, AJ, 133, 734
Bloom, J. S., Perley, D. A., Li, W., et al. 2009, ApJ, 691, 723
Bohlin, R. C., & Gilliland, R. L. 2004, AJ, 127, 3508
Bouché, N., Murphy, M. T., Péroux, C., et al. 2012, MNRAS, 419, 2
Bruzual, G., & Charlot, S. 2003, MNRAS, 344, 1000
Calzetti, D., Armus, L., Bohlin, R. C., et al. 2000, ApJ, 533, 682
Cardelli, J. A., Clayton, G. C., & Mathis, J. S. 1989, ApJ, 345, 245
Carswell, R. F., Whelan, J. A. J., Smith, M. G., Boksenberg, A., & Tytler, D. 1982, MNRAS, 198, 91

Chabrier, G., Baraffe, I., Allard, F., & Hauschildt, P. 2000, ApJ, 542, 464
Chandra, P., & Frail, D. A. 2012, ApJ, 746, 156
Chen, H.-W. 2012, MNRAS, 419, 3039
Chen, H., & Lanzetta, K. M. 2003, ApJ, 597, 706
Chen, H.-W., Lanzetta, K. M., & Fernández-Soto, A. 2000, ApJ, 533, 120
Chen, H., Prochaska, J. X., Bloom, J. S., & Thompson, I. B. 2005, ApJ, 634, L25
Chen, H., Perley, D. A., Pollack, L. K., et al. 2009, ApJ, 691, 152
Chen, H.-W., Helsby, J. E., Gauthier, J.-R., et al. 2010, ApJ, 714, 1521
Christensen, L., Sánchez, S. F., Jahnke, K., et al. 2004a, Astron. Nachr., 325, 124
Christensen, L., Sánchez, S. F., Jahnke, K., et al. 2004b, A&A, 417, 487
Coppolani, F., Petitjean, P., Stoehr, F., et al. 2006, MNRAS, 370, 1804
Courbin, F., Magain, P., Kirkove, M., & Sohy, S. 2000, ApJ, 529, 1136
Dahlen, T., Mobasher, B., Somerville, R. S., et al. 2005, ApJ, 631, 126
Dall'Aglio, A., Wisotzki, L., & Worseck, G. 2009, ApJ, submitted [arXiv:0906.1484]
Devillard, N. 1997, The Messenger, 87, 19
Djorgovski, S. G., Pahre, M. A., Bechtold, J., & Elston, R. 1996, Nature, 382, 234
D'Odorico, V., Petitjean, P., & Cristiani, S. 2002, A&A, 390, 13
Ellison, S. L. 2006, MNRAS, 368, 335
Ellison, S. L., Yan, L., Hook, I. M., et al. 2002, A&A, 383, 91
Ellison, S. L., Ibata, R., Pettini, M., et al. 2004, A&A, 414, 79
Ellison, S. L., Vreeswijk, P., Ledoux, C., et al. 2006, MNRAS, 372, L38
Ellison, S. L., Hennawi, J. F., Martin, C. L., & Sommer-Larsen, J. 2007, MNRAS, 378, 801
Ellison, S. L., Murphy, M. T., & Dessauges-Zavadsky, M. 2009, MNRAS, 392, 998
Ellison, S. L., Prochaska, J. X., Hennawi, J., et al. 2010, MNRAS, 406, 1435
Faucher-Giguère, C., Lidz, A., Zaldarriaga, M., & Hernquist, L. 2008, ApJ, 673, 39
Fazio, G. G., Hora, J. L., Allen, L. E., et al. 2004, ApJS, 154, 10
Fox, A. J., Petitjean, P., Ledoux, C., & Srianand, R. 2007, A&A, 465, 171
Fox, A. J., Ledoux, C., Vreeswijk, P. M., Smette, A., & Jaunsen, A. O. 2008, A&A, 491, 189
Francis, P. J., & Hewett, P. C. 1993, AJ, 105, 1633
Francis, P. J., Woodgate, B. E., Warren, S. J., et al. 1996, ApJ, 457, 490
Fumagalli, M., O'Meara, J. M., Prochaska, J. X., & Kanekar, N. 2010, MNRAS, 408, 362
Fynbo, J. U., Møller, P., & Warren, S. J. 1999, MNRAS, 305, 849
Fynbo, J. P. U., Ledoux, C., Møller, P., Thomsen, B., & Burud, I. 2003, A&A, 407, 147
Fynbo, J. P. U., Starling, R. L. C., Ledoux, C., et al. 2006, A&A, 451, L47
Fynbo, J. P. U., Prochaska, J. X., Sommer-Larsen, J., Dessauges-Zavadsky, M., & Møller, P. 2008, ApJ, 683, 321
Fynbo, J. P. U., Jakobsson, P., Prochaska, J. X., et al. 2009, ApJS, 185, 526
Fynbo, J. P. U., Laursen, P., Ledoux, C., et al. 2010, MNRAS, 408, 2128
Fynbo, J. P. U., Ledoux, C., Noterdaeme, P., et al. 2011, MNRAS, 413, 2481
Giavalisco, M. 2002, ARA&A, 40, 579
Gonzalez Delgado, R. M., Leitherer, C., Heckman, T., et al. 1998, ApJ, 495, 698
Greiner, J., Krühler, T., Klose, S., et al. 2011, A&A, 526, A30
Guimarães, R., Petitjean, P., Rollinde, E., et al. 2007, MNRAS, 377, 657
Haehnelt, M. G., Steinmetz, M., & Rauch, M. 1998, ApJ, 495, 647
Hennawi, J. F., & Prochaska, J. X. 2007, ApJ, 655, 735
Henriksen, C. 2008, Master's Thesis, DARK Cosmology Center – Niels Bohr Institute, Copenhagen University, Juliane Maries Vej 30, 2100 Copenhagen, ø Denmark
Hjorth, J., & Bloom, J. S. 2011 [arXiv:1104.2274]
Hjorth, J., Malesani, D., Jakobsson, P., et al. 2012, ApJ, 756, 187
Ilbert, O., Arnouts, S., McCracken, H. J., et al. 2006, A&A, 457, 841
Jakobsson, P., Hjorth, J., Fynbo, J. P. U., et al. 2004, A&A, 427, 785
Jimenez, R., Bowen, D. V., & Matteucci, F. 1999, ApJ, 514, L83
Kann, D. A., Klose, S., Zhang, B., et al. 2010, ApJ, 720, 1513
Kouveliotou, C., Meegan, C. A., Fishman, G. J., et al. 1993, ApJ, 413, L101
Krist, J. 1993, in Astronomical Data Analysis Software and Systems II, eds. R. J. Hanisch, R. J. V. Brissenden, & J. Barnes, ASP Conf. Ser., 52, 536
Krogager, J.-K., Fynbo, J. P. U., Møller, P., et al. 2012, MNRAS, L461
Krühler, T., Greiner, J., Schady, P., et al. 2011, A&A, 534, A108
Kunth, D., Mas-Hesse, J. M., Terlevich, E., et al. 1998, A&A, 334, 11
Landolt, A. U. 1992, AJ, 104, 340
Larson, D., Dunkley, J., Hinshaw, G., et al. 2011, ApJS, 192, 16
Laursen, P., Sommer-Larsen, J., & Andersen, A. C. 2009, ApJ, 704, 1640
Le Brun, V., Bergeron, J., Boisse, P., & Deharveng, J. M. 1997, A&A, 321, 733
Ledoux, C., Vreeswijk, P., Ellison, S., et al. 2005, GCN Circ., 3860
Ledoux, C., Vreeswijk, P. M., Smette, A., et al. 2009, A&A, 506, 661
Letawe, Y., Magain, P., Letawe, G., Courbin, F., & Hutsemékers, D. 2008, ApJ, 679, 967
Lu, L., Wolfe, A. M., Turnshek, D. A., & Lanzetta, K. M. 1993, ApJS, 84, 1
Magain, P., Courbin, F., & Sohy, S. 1998, ApJ, 494, 472
Markwardt, C. B. 2009, in Astronomical Data Analysis Software and Systems XVIII, eds. D. A. Bohlender, D. Durand, & P. Dowler, ASP Conf. Ser., 411, 251
Masetti, N., Palazzi, E., Pian, E., et al. 2003, A&A, 404, 465
Møller, P., & Warren, S. J. 1993, A&A, 270, 43
Møller, P., Warren, S. J., Fall, S. M., Fynbo, J. U., & Jakobsen, P. 2002, ApJ, 574, 51
Møller, P., Fynbo, J. P. U., & Fall, S. M. 2004, A&A, 422, L33
Milvang-Jensen, B., Fynbo, J. P. U., Malesani, D., et al. 2012, ApJ, 756, 25
Nagamine, K., Wolfe, A. M., Hernquist, L., & Springel, V. 2007, ApJ, 660, 945
Noterdaeme, P., Petitjean, P., Ledoux, C., & Srianand, R. 2009, A&A, 505, 1087
Noterdaeme, P., Laursen, P., Petitjean, P., et al. 2012, A&A, 540, A63
Okoshi, K., & Nagashima, M. 2005, ApJ, 623, 99
Overzier, R. A., Heckman, T. M., Schiminovich, D., et al. 2010, ApJ, 710, 979
Pâris, I., Petitjean, P., Rollinde, E., et al. 2011, A&A, 530, A50
Péroux, C., Dessauges-Zavadsky, M., D'Odorico, S., Sun Kim, T., & McMahon, R. G. 2005, MNRAS, 363, 479
Péroux, C., Bouché, N., Kulkarni, V. P., York, D. G., & Vladilo, G. 2011, MNRAS, 410, 2237
Péroux, C., Bouché, N., Kulkarni, V. P., York, D. G., & Vladilo, G. 2012, MNRAS, 419, 3060
Petry, C. E., Impey, C. D., & Foltz, C. B. 1998, ApJ, 494, 60
Pettini, M., Kellogg, M., Steidel, C. C., et al. 1998a, ApJ, 508, 539
Pettini, M., Steidel, C. C., Adelberger, K. L., et al. 1998b, in ASP Conf. Ser., 148, Origins, eds. C. E. Woodward, J. M. Shull, & H. A. Thronson Jr., 67
Pettini, M., Steidel, C. C., Adelberger, K. L., Dickinson, M., & Giavalisco, M. 2000, ApJ, 528, 96
Piranomonte, S., Ward, P. A., Fiore, F., et al. 2008, A&A, 492, 775
Pollack, L. K., Chen, H., Prochaska, J. X., & Bloom, J. S. 2009, ApJ, 701, 1605
Prochaska, J. X., & Wolfe, A. M. 1997, ApJ, 487, 73
Prochaska, J. X., & Wolfe, A. M. 1998, ApJ, 507, 113
Prochaska, J. X., & Wolfe, A. M. 2009, ApJ, 696, 1543
Prochaska, J. X., Herbert-Fort, S., & Wolfe, A. M. 2005, ApJ, 635, 123
Prochaska, J. X., Chen, H., Bloom, J. S., et al. 2007a, ApJS, 168, 231
Prochaska, J. X., Chen, H., Dessauges-Zavadsky, M., & Bloom, J. S. 2007b, ApJ, 666, 267
Prochaska, J. X., Chen, H.-W., Wolfe, A. M., Dessauges-Zavadsky, M., & Bloom, J. S. 2008, ApJ, 672, 59
Prochter, G. E., Prochaska, J. X., & Burles, S. M. 2006, ApJ, 639, 766
Racusin, J. L., Liang, E. W., Burrows, D. N., et al. 2009, ApJ, 698, 43
Rafelski, M., Wolfe, A. M., & Chen, H.-W. 2011, ApJ, 736, 48
Rao, S. M., & Turnshek, D. A. 2000, ApJS, 130, 1
Rao, S. M., Belfort-Mihalyi, M., Turnshek, D. A., et al. 2011, MNRAS, 416, 1215
Rauch, M. 1998, ARA&A, 36, 267
Reddy, N. A., Steidel, C. C., Pettini, M., et al. 2008, ApJS, 175, 48
Rollinde, E., Srianand, R., Theuns, T., Petitjean, P., & Chand, H. 2005, MNRAS, 361, 1015
Russell, D. M., Ellison, S. L., & Benn, C. R. 2006, MNRAS, 367, 412
Salvaterra, R., Della Valle, M., Campana, S., et al. 2009, Nature, 461, 1258
Schady, P., Page, M. J., Oates, S. R., et al. 2010, MNRAS, 401, 2773
Sirianni, M., Jee, M. J., Benítez, N., et al. 2005, PASP, 117, 1049
Smette, A., Robertson, J. G., Shaver, P. A., et al. 1995, A&AS, 113, 199
Smith, H. E., Cohen, R. D., Burns, J. E., Moore, D. J., & Uchida, B. A. 1989, ApJ, 347, 87
Starling, R. L. C., Vreeswijk, P. M., Ellison, S. L., et al. 2005, A&A, 442, L21
Steidel, C. C., Adelberger, K. L., Giavalisco, M., Dickinson, M., & Pettini, M. 1999, ApJ, 519, 1
Stetson, P. B. 2000, PASP, 112, 925
Tanvir, N. R., Fox, D. B., Levan, A. J., et al. 2009, Nature, 461, 1254
Tody, D. 1986, in SPIE Conf. Ser. 627, ed. D. L. Crawford, 733
Tyson, N. D. 1988, ApJ, 329, L57
Tytler, D. 1987, ApJ, 321, 69
Vergani, S. D., Petitjean, P., Ledoux, C., et al. 2009, A&A, 503, 771
Verhamme, A., Schaerer, D., & Maselli, A. 2006, A&A, 460, 397
Vreeswijk, P. M., Møller, P., & Fynbo, J. P. U. 2003, A&A, 409, L5
Vreeswijk, P. M., Ellison, S. L., Ledoux, C., et al. 2004, A&A, 419, 927
Warren, S. J., Møller, P., Fall, S. M., & Jakobsen, P. 2001, MNRAS, 326, 759
Weatherley, S. J., Warren, S. J., Møller, P., et al. 2005, MNRAS, 358, 985
Wolfe, A. M. 1986, Roy. Soc. London Philos. Trans. Ser. A, 320, 503
Wolfe, A. M., & Prochaska, J. X. 1998, ApJ, 494, L15
Wolfe, A. M., Gawiser, E., & Prochaska, J. X. 2005, ARA&A, 43, 861
Woosley, S. E. 2011 [arXiv:1105.4193]
Zafar, T., Watson, D., Fynbo, J. P. U., et al. 2011, A&A, 532, A143
Zhang, B., & Mészáros, P. 2004, Int. J. Mod. Phys. A, 19, 2385